Geomorphology 297 (2017) 20–42

Contents lists available at ScienceDirect

Geomorphology

journal homepage: www.elsevier.com/locate/geomorph

Degradation and stabilization of ice wedges: Implications for assessing risk of thermokarst in northern Alaska

Mikhail Kanevskiy [a,*], Yuri Shur [a], Torre Jorgenson [a,b], Dana R.N. Brown [c], Nataliya Moskalenko [d], Jerry Brown [e], Donald A. Walker [c], Martha K. Raynolds [c], Marcel Buchhorn [c,f]

[a] Institute of Northern Engineering, University of Alaska Fairbanks, Fairbanks, AK, USA
[b] Alaska Ecoscience, Fairbanks, AK, USA
[c] Institute of Arctic Biology, University of Alaska Fairbanks, AK, USA
[d] Earth Cryosphere Institute, Moscow, Russia
[e] Falmouth, MA, USA
[f] Flemish Institute for Technological Research (VITO), Mol, Belgium

ARTICLE INFO

Article history:
Received 13 May 2017
Received in revised form 31 August 2017
Accepted 1 September 2017
Available online 14 September 2017

Dedicated to the memory of Dr. Tamara Zhestkova.

Keywords:
Permafrost
Ground ice
Frozen soils
Intermediate layer

ABSTRACT

Widespread degradation of ice wedges has been observed during the last decades in numerous areas within the continuous permafrost zone of Eurasia and North America. To study ice-wedge degradation, we performed field investigations at Prudhoe Bay and Barrow in northern Alaska during 2011–2016. In each study area, a 250-m transect was established with plots representing different stages of ice-wedge degradation/stabilization. Field work included surveying ground- and water-surface elevations, thaw-depth measurements, permafrost coring, vegetation sampling, and ground-based LiDAR scanning. We described cryostratigraphy of frozen soils and stable isotope composition, analyzed environmental characteristics associated with ice-wedge degradation and stabilization, evaluated the vulnerability and resilience of ice wedges to climate change and disturbances, and developed new conceptual models of ice-wedge dynamics that identify the main factors affecting ice-wedge degradation and stabilization and the main stages of this quasi-cyclic process. We found significant differences in the patterns of ice-wedge degradation and stabilization between the two areas, and the patterns were more complex than those previously described because of the interactions of changing topography, water redistribution, and vegetation/soil responses that can interrupt or reinforce degradation. Degradation of ice wedges is usually triggered by an increase in the active-layer thickness during exceptionally warm and wet summers or as a result of flooding or disturbance. Vulnerability of ice wedges to thermokarst is controlled by the thickness of the intermediate layer of the upper permafrost, which overlies ice wedges and protects them from thawing. In the continuous permafrost zone, degradation of ice wedges rarely leads to their complete melting; and in most cases wedges eventually stabilize and can then resume growing, indicating a somewhat cyclic and reversible process. Stabilization of ice wedges after their partial degradation makes them better protected than before degradation because the intermediate layer is usually 2 to 3 times thicker on top of stabilized ice wedges than on top of initial ice wedges in undisturbed conditions. As a result, the likelihood of formation of large thaw lakes in the continuous permafrost zone triggered by ice-wedge degradation alone is very low.

1. Introduction

Widespread degradation of ice wedges has been observed in various permafrost regions of Eurasia and North America during the last decades, mostly in areas of cold continuous permafrost (Jorgenson et al., 2006, 2015; Liljedahl et al., 2016). Ice-wedge degradation strongly affects the environment, including topography, hydrology, vegetation and soils, and infrastructure and thus is expected to have large consequences for northern regions. Thermokarst pits and troughs in polygonal terrain are one of the most characteristic thermokarst landforms resulting from thawing of ice-rich permafrost containing ice wedges (Shur and Osterkamp, 2007; Jorgenson et al., 2008; Kokelj and Jorgenson, 2013).

Ice wedges, and their associated polygonal topography, occur nearly everywhere in the Arctic and wedge ice is considered to be the most common type of massive ground ice (Leffingwell, 1915; Mackay, 1972; Vtyurin, 1975; French and Shur, 2010; Murton, 2013). Along the Beaufort Sea coast of Alaska, the width of mainly epigenetic ice wedges varied from several centimeters to >5 m, while their vertical extent usually did not exceed 4 m (Kanevskiy et al., 2013). The size of ice-wedge

* Corresponding author at: 233 Duckering Bldg., P.O. Box 755910, Fairbanks, AK 99775-5910, USA.
E-mail address: mkanevskiy@alaska.edu (M. Kanevskiy).

http://dx.doi.org/10.1016/j.geomorph.2017.09.001
0169-555X/

polygons varied from <10 to >20 m across, with the largest polygons occurring in drained-lake basins, deltas, and tidal flats. Brown (1968) estimated wedge-ice volume in the Barrow study area and assumed that the average number (10%) was representative for the entire Arctic Coastal Plain. Kanevskiy et al. (2013) estimated that the average volumetric content of wedge ice near the Beaufort Sea coast was 11%, but at some locations it exceeded 50%, and that the average total volumetric ice content (including wedge, segregated, and pore ice) in the upper 3 m of permafrost was 77%. Everett (1980a) estimated the volume of wedge ice in the wall of 2.2-m-deep and 100-m-long trench at the experimental gas pipeline test site at Prudhoe Bay to be ~40%. In the adjacent Prudhoe Bay study area, Jorgenson et al. (2015) estimated the volume of wedge ice in the upper 3 m to be 21%. Pollard and French (1980) estimated ice-wedge volume in the upper 4.5 m to be 12–16% for the Mackenzie Delta. Recent advances in the study of structure and dynamics of ice wedges were reviewed by Christiansen et al. (2016).

Recent thermokarst-related changes in polygonal terrain have been studied in Alaska (Jorgenson et al., 2006, 2015; Liljedahl et al., 2012, 2016; Necsoiu et al., 2013; Frost et al., 2014; Raynolds et al., 2014; Walker et al., 2014, 2015; Jones et al., 2015; Lara et al., 2015; Abolt et al., 2016; Farquharson et al., 2016; Kanevskiy et al., 2016; Swanson, 2016), Canada (Fortier et al., 2007; Kershaw, 2008; Gamon et al., 2012; Godin et al., 2014; Kokelj et al., 2014; Pollard et al., 2015; Liljedahl et al., 2016; Steedman et al., 2017; Wolter et al., 2016), and Russia (Minke et al., 2009; de Klerk et al., 2011; Fedorov et al., 2012; Helbig et al., 2013; Sejourne et al., 2015; Liljedahl et al., 2016), but only in several of these studies have data on frozen soils and ground ice structure and properties been presented (Jorgenson et al., 2006, 2015; Fortier et al., 2007; Kokelj et al., 2014; Pollard et al., 2015; Walker et al., 2015; Kanevskiy et al., 2016). Changes in the extent of ice-wedge thermokarst, as indicated by water-filled troughs, have shown rapid increases during the last couple of decades (Jorgenson et al., 2006, 2015; Necsoiu et al., 2013; Frost et al., 2014; Raynolds et al., 2014; Swanson, 2016; Steedman et al., 2017). Methods and results of recent remote sensing studies on ice-wedge thermokarst were summarized by Jorgenson and Grosse (2016).

Processes of ice-wedge thermokarst and thermo-erosion are often associated with formation of thermokarst-cave ice. The term *thermokarst-cave ice* (TCI) was suggested by Shumskii (1959) for massive ice formed by the freezing of water trapped in underground cavities that were cut into permafrost by running water. In Canada, this type of ice was described as *pool ice* by Mackay (1997, 2000). The TCI bodies usually form within and next to ice wedges and are oriented horizontally. They are composed of ice that is mostly clean, are colorless to yellowish from dissolved organics, and contain irregularly distributed air bubbles; and frequently are underlain by sediment-rich *basal* ice layer and/or ice-rich soil with reticular-chaotic cryostructure (Shur et al., 2004; Bray et al., 2006; Fortier et al., 2008; Kanevskiy et al., 2008). The TCI can be easily recognized in boreholes or exposures because it does not have the distinctive vertical foliation typical of wedge ice. Maximum thickness of TCI bodies exposed on the Beaufort Sea coast reached up to 120 cm, and their visible lateral extent reached up to 5 m. Our measurements at the 600-m-long and 7- to 10-m-high coastal exposure near Kaktovik showed that the TCI bodies occupied ~2% of the face of the bluff (Kanevskiy et al., 2013).

Previous studies in northern Alaska (Jorgenson et al., 2006, 2015) showed that degradation of ice wedges is a reversible process, which includes five main stages: undegraded ice wedges (UD: narrow troughs, well vegetated), degradation initial (DI: narrow troughs with shallow flooding, D1 in this paper), degradation advanced (DA: wide troughs, deeply flooded, D2 in this paper), stabilization initial (SI: wide troughs, shallowly flooded), and stabilization advanced (SA: wide troughs, surface above the water table). According to a conceptual model of ice-wedge dynamics (Jorgenson et al., 2015), initial degradation is caused by extreme weather conditions (e.g., exceptionally warm and wet summers) or physical disturbance, which leads to deepening of the active layer and partial thawing of ice wedges. During the advanced degradation stage, water impoundment causes energy balance changes, which lead to further thawing of ice wedges. Initial stabilization of degraded ice wedges starts as a result of development of aquatic vegetation in thermokarst troughs and pits, which causes decreases in active-layer thickness and formation of a new intermediate layer (Shur et al., 2011) above the ice wedges. Eventually, slumping of materials from the banks of troughs, continued vegetation growth, organic matter accumulation, ground-ice aggradation, and heaving of the surface result in draining of ice-wedge troughs (advanced stabilization). A thick intermediate layer at this stage protects the remnant ice wedges from future degradation.

Raynolds et al. (2014) described two scenarios for ice-wedge thermokarst in the areas of ice-rich permafrost: reversible and irreversible. (Under natural conditions, degrading wedges can easily recover (time of recovery depends on a depth of thaw subsidence). When anthropogenic disturbance causes destruction of vegetation and removal of the organic-rich soils, more severe degradation may occur; and a possibility exists that small initial thermokarst features can evolve into thaw lakes. The stages of transformation of small thermokarst pits and troughs into large thaw lakes have been described in numerous papers (Hopkins, 1949; Britton, 1957; Soloviev, 1962; Hussey and Michelson, 1966; Tomirdiaro, 1972; Czudek and Demek, 1973; Billings and Peterson, 1980; Everett, 1980b; Hinkel et al., 2003; Shur et al., 2012). However, this potential transformation has been described mainly theoretically, and in reality it may be more complicated. For example, ice-wedge thermokarst caused by heavy disturbance (removal of vegetation and surficial peat) many decades ago in the continuous permafrost zone has not resulted in thaw-lake formation (Lawson, 1986; Shur, 1988a).

In this study, we examine processes affecting ice-wedge degradation to better understand ice wedges' likely response to climate change and disturbance. Given the complexity of ground-ice dynamics and interacting environmental factors, the patterns and processes of ice-wedge evolution described in the earlier models need further evaluation. The objectives of this paper are to (i) compare ground ice, soil stratigraphy, stable isotopes, and environmental characteristics across terrain with varying ice-wedge conditions based on our field investigations performed in 2011 – 2016 at Prudhoe Bay and Barrow in northern Alaska; (ii) improve upon earlier conceptual models of the patterns and stages associated with ice-wedge dynamics and identify the main factors affecting ice-wedge degradation and stabilization; (iii) develop a risk assessment approach for evaluating the vulnerability and resilience of ice wedges to climate change and disturbances; and (iv) evaluate the likelihood of ice-wedge degradation progressing to thaw-lake development.

2. Study areas

Our study areas at Prudhoe Bay (PB) and Barrow (BW) are situated on the Arctic Coastal Plain close to the Beaufort Sea coast of Alaska (BSCA) (Fig. 1). The PB study area (N70.229° W148.419°) was described in detail by Jorgenson et al. (2015), who interpreted it as an old drained-lake basin. This interpretation is challenged by Walker who described the same area as a residual surface of the ancient floodplain of the Sagavanirktok River, unmodified by thaw-lake processes (Walker et al., 2015). Soils, landscapes, and vegetation in the larger Prudhoe Bay area were described by Everett (1980a, 1980b), Walker et al. (1980), Walker (1985), and Walker and Everett (1991). Environmental changes caused by infrastructure impacts in the Prudhoe Bay Oil Field, including thermokarst development, were analyzed by Walker et al. (1980, 1987, 2014) and Raynolds et al. (2014).

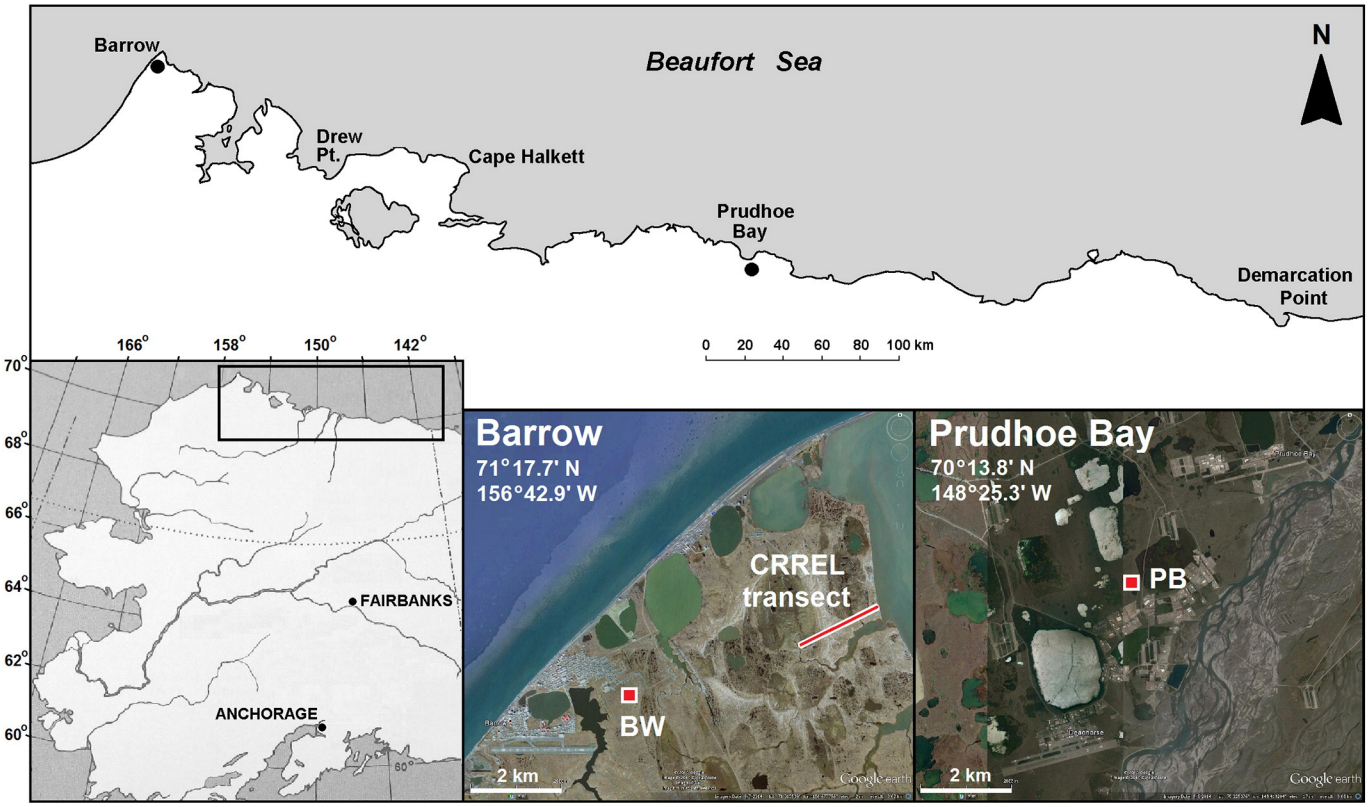

Fig. 1. Locations of study areas.

The BW study area (N71.295° W156.714°) is located near the tunnel excavated in the 1960s (Fig. S1), which revealed a system of large pre-Holocene buried ice wedges (Brown, 1965; Meyer et al., 2010). This area belongs to the primary (or initial) surface of the Arctic Coastal Plain, which has not been reworked by thaw-lake processes through the Holocene (O'Sullivan, 1961; Brown, 1965; Hussey and Michelson, 1966). In the shaft of this tunnel, silts and silty very fine sands with ~30-cm-thick peat layer (from 0.5 to 0.8 m), occasional gravel inclusions, and numerous peat inclusions (mainly at depths of 1.3 − 1.7 and 3.2 − 3.4 m) were exposed above the buried ice wedges (observed from ~3.4 m). Gravimetric moisture contents of soils with mainly ataxitic cryostructure varied from 55 to 200% and averaged 102.9% (Jorgenson, 2011; Kanevskiy et al., 2013). At a depth of ~7 m, sandy silts are underlain by saline gravelly sands (Meyer et al., 2010). Brown (1967) suggested that pre-Holocene ice wedges in the tunnel area melted in the early Holocene to the 3-m depth, which caused accumulation of surface peat in more favorable wetter conditions. Subsequent refreezing of thawed soils was accompanied by accumulation of excess ice and formation of a new generation of ice wedges, which are still active. For this study, we also use the data obtained from the 2.1-km-long CRREL transect (Fig. 1), which was established in 1962 near Barrow between Elson Lagoon on the east and the drainage of central Marsh Creek on the west; elevations along this transect varied from 0.8 to 5.0 m asl and were significantly lower than at BW (Brown and Johnson, 1965; Brown, 1969).

Both study areas are characterized by the Arctic climate with long and cold winters, low precipitation, and strong winds. Climate conditions are similar along the BSCA, with a mean annual air temperature (MAAT) of ~ −11 °C, annual precipitation <150 mm, and annual snowfall <100 cm (Alaska Climate Research Center, Climate Normals, 1981−2010). Climate in Barrow is characterized by colder summers and warmer winters in comparison with Prudhoe Bay.

The BSCA is a lowland with a relatively flat surface. Most coastal bluffs are 2 − 5 m high. The surficial deposits of this area include Quaternary sediments of various origins (fluvial, marine, eolian, deltaic), significantly modified by thermokarst, lacustrine, and paludification processes, resulting in an abundance of lake-basin deposits (Brown and Sellmann, 1973; Rawlinson, 1993; Jorgenson, 2011). As a result of accumulation of ground ice in drained lake basins, the amount of segregated and wedge ice in mature basins is very similar to that of the primary surface of the Arctic Coastal Plain (Kanevskiy et al., 2013).

The BSCA is the area of cold continuous permafrost. Permafrost thickness generally varies from 200 to 400 m, but in the Prudhoe Bay area it exceeds 600 m (Gold and Lachenbruch, 1973; Lachenbruch et al., 1988; Jorgenson, 2011). Mean annual ground temperature (MAGT) of permafrost strongly depends on local conditions and varies between −5 and −10 °C; during the last decades, a significant increase in MAGT has been reported (Smith et al., 2010; Jorgenson, 2011; Romanovsky et al., 2016). The active layer thickness (ALT) varies depending on local conditions from about 20 cm in thick peat to >100 cm in poorly vegetated sand dunes. The ALT on gravelly south-facing slopes of pingos exceeds 140 cm (Walker, 1990). Despite a recent increase in MAAT and MAGT, a slight decreasing trend in the ALT has been reported during the last decades for 10 sites on the Alaskan Coastal Plain; these records also indicate significant –– up to 15% above the long-term mean value (which was 0.45 m in 1995–2011) –– increase in the mean ALT in 1998, 2004, 2006, and 2011 (Streletskiy et al., 2008; Shiklomanov et al., 2012). At Barrow, the ALT measurements showed large interannual variability but no clear trend from 1995 to 2014 (Brown et al., 2015). Despite a lack of increasing trend, a significant (up to 1 cm/y) subsidence of the ground surface within the four plots located along the CRREL transect was observed in 2003–2015; it may be attributed mainly to thawing of ice wedges (Streletskiy et al., 2016).

The coastal area is characterized by extremely high ground-ice content of the upper permafrost (Leffingwell, 1919; Hussey and Michelson,

1966; Brown and Sellmann, 1973; Sellmann et al., 1975; Everett, 1980a; Black, 1983; Jorgenson, 2011; Bockheim and Hinkel, 2012; Kanevskiy et al., 2013). Ground ice exists in two main forms: (i) massive ground ice, and (ii) pore and segregated ice, forming cryostructures. In the BSCA region, four main types of massive ground ice have been distinguished: (i) ice wedges, (ii) thermokarst-cave ice, (iii) ice cores of pingos, and (iv) folded massive ice of presumably glacial origin (Kanevskiy et al., 2013). During this study, only two types of massive ground ice were detected in the Prudhoe Bay and Barrow study areas: wedge ice and thermokarst-cave ice.

3. Methods

3.1. Sampling strategy

In the PB and BW study areas, 250-m transects were established in early June 2011 (Fig. 2) and late July–early August 2012 (Fig. 3), correspondingly. Along each transect, 18 plots representing five stages of ice-wedge degradation/stabilization and centers of ice-wedge polygons (Jorgenson et al., 2015) were established. Additional plots/coring locations were located off the transects to obtain more data for some stages. Work included surveying ground- and water-surface elevations, permafrost coring for soil stratigraphy and ground-ice descriptions, thaw-depth measurements, vegetation sampling, and ground-based LiDAR scanning to develop a high-resolution DEM. We also analyzed the photographs of frozen cores from 80 boreholes within 20 plots representing various terrain units, which had been sampled in spring 1963 along the 2.1-km-long CRREL transect located near Barrow (Fig. 1) (Brown and Johnson, 1965; Brown, 1969).

3.2. Soil, ground ice, and stable isotopes

To study frozen soil and ground ice, 167 boreholes up to 4 m deep were drilled with a SIPRE corer (7.5 and 5.0 cm in diameter). In PB, 56 boreholes were drilled in early June 2011 and 57 boreholes in late July 2012 (a total of 113 boreholes); in BW, 54 boreholes were drilled in late July–early August 2012. Some of these boreholes were drilled across ice wedges to evaluate ice-wedge dimensions. Massive ground-ice bodies and cryostructures (patterns formed by ice inclusions in the frozen soil) were described using classifications adapted from Russian and North American literature (French and Shur, 2010; Kanevskiy et al., 2013). More than 180 core samples (94 in PB, 90 in BW) were taken to estimate gravimetric and volumetric moisture contents (GMC and VMC).

To estimate ice-wedge content, we used methods described by Kanevskiy et al. (2013) and Jorgenson et al. (2015). To estimate ice-wedge length, the center lines of ice-wedge troughs were manually interpreted and delineated on high-resolution imagery for PB (14 July 2009) and BW (GeoEye 11 July 2012) using ArcMap software (ESRI,

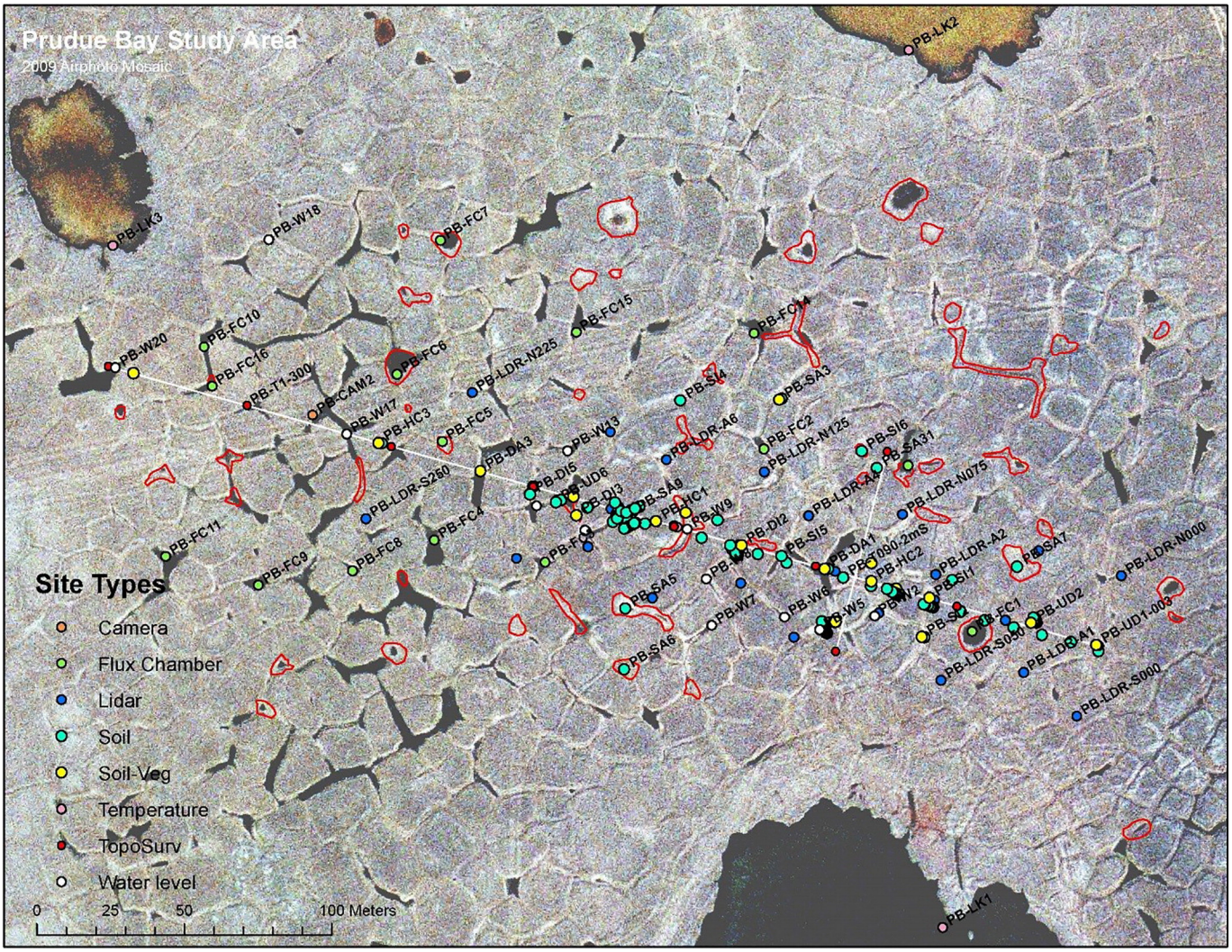

Fig. 2. Prudhoe Bay (PB) study area: location of the transect and sampling sites projected on 2009 airphoto, with 1982 waterbodies outlined in red.

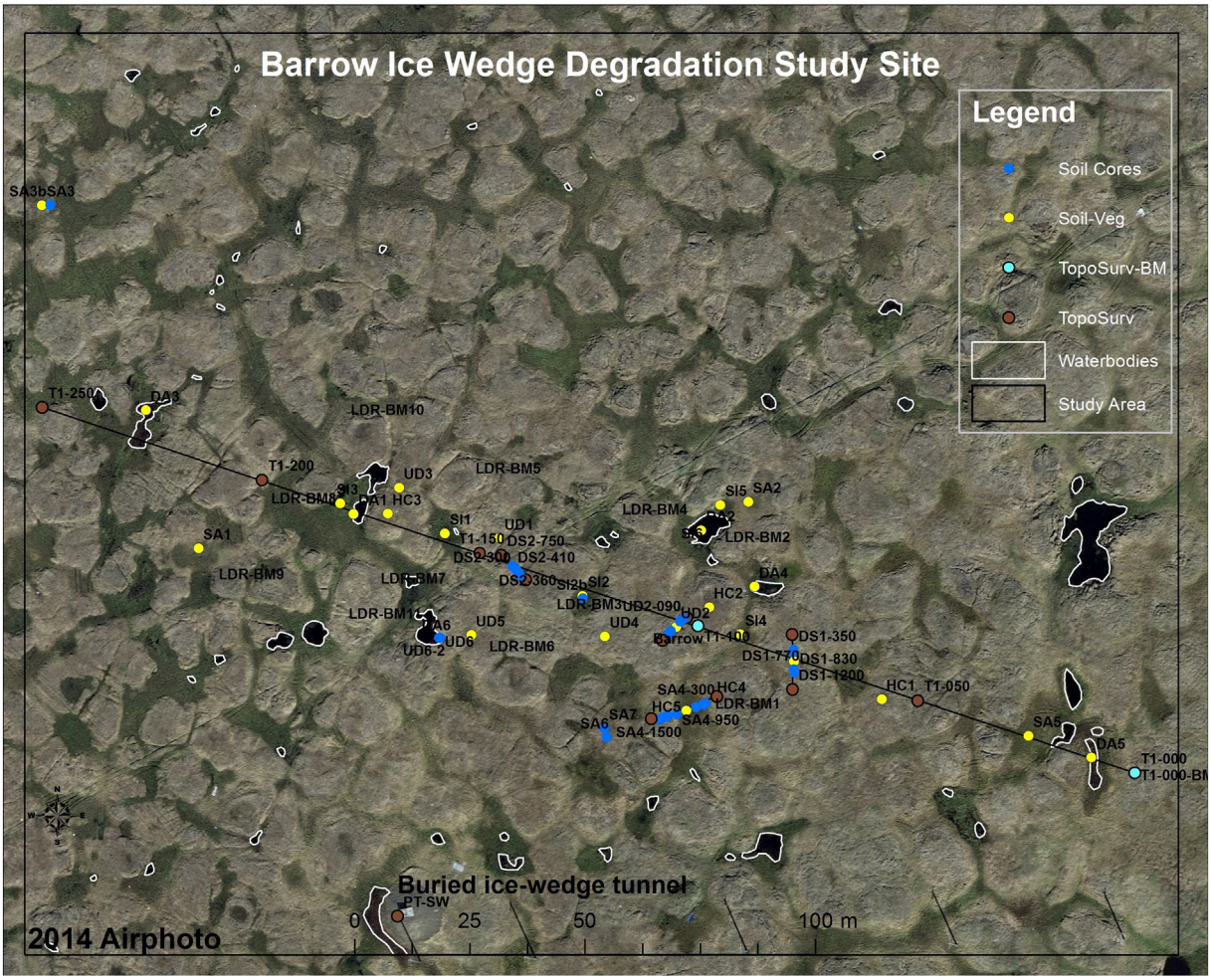

Fig. 3. Barrow (BW) study area: location of sampling sites along the transect.

Redlands, CA). Waterbodies were also delineated during the interpretation. The length of the segments within three 1-ha areas were then totaled. We estimated ice-wedge cross section dimensions from the coring profiles. Volume was then calculated as length × cross-sectional area.

For oxygen and hydrogen isotopic composition ($\delta^{18}O$ and $\delta^{2}H$), samples of different types of ground ice and surface water were analyzed at the Alaska Stable Isotope Facility at the University of Alaska Fairbanks using standard mass spectrometry method. Stable hydrogen and oxygen isotopic compositions were expressed as delta values in per mil (‰) relative to the Vienna Standard Mean Ocean Water (VSMOW). The results are presented by relating $\delta^{18}O$ and $\delta^{2}H$ values to the Global Meteoric Water Line (GMWL) (Craig, 1961). The lowest $\delta^{18}O$ and $\delta^{2}H$ values correspond to the coldest temperatures at the time of ice formation. Radiocarbon dating was performed by the National Ocean Sciences AMS Facility, Woods Hole Oceanographic Institution, on seven samples obtained from the BW study area.

3.3. Environmental factors

Environmental factors evaluated during our study included microtopography, water and snow depths, depths of seasonal thaw, air and soil temperatures, and vegetation. Ground- and water-surface elevations were measured with 1-m spacing along 250-m transects using an autolevel and rod at 1-cm resolution. Thaw depths were measured every 1 m to the nearest 1 cm and used to calculate permafrost table elevations. Detailed microtopography surveys were performed using ground-based LiDAR scanning with a laser scanner (IS 3″ Image Station, Topcon, Inc.). Additionally, in the PB study area, ground-surface elevations, water levels, snow depths, and air and soil temperatures were measured periodically; methods were described by Jorgenson et al. (2015).

Vegetation cover at both study areas was described at the 18 intensive plots using the point-intercept method. Plots had variable sizes (5 m long by 0.4, 1, or 2 m wide) to accommodate the varying width of the troughs. At 100 points per plot, the first occurrence of each species intercepted by a laser pointer was recorded, thus each hit had a value of 1% cover. After point sampling, the plots were examined for additional species and a trace value (0.1%) assigned to species that were present but not captured in the point sampling. For the purposes of this study, we report only the dominant species that are associated with each stage of ice-wedge degradation/stabilization and use the nomenclature of the PLANTS Database (https://plants.usda.gov) of the Natural Resource Conservation Service (USDA).

3.4. Development of conceptual model

To integrate and synthesize the variability in the data and patterns we observed, we developed a new conceptual model of ice-wedge degradation and stabilization that illustrates ice-wedge spatial relationships with the active layer and the upper permafrost, surface topography, and vegetation. The cross-sectional diagrams illustrate how these properties vary with the various degradation and stabilization phases. For each stage, we estimate or describe the duration of the stage (years), water depths, ice-wedge and thermokarst-cave ice characteristics, thickness of the intermediate layer, and dominant vegetation.

3.5. Risk analysis

Estimation of a risk of ice-wedge degradation is based on evaluation of thickness and properties of soil layers overlying ice wedges (Kanevskiy et al., 2016), which include active, transient, and intermediate layers. The transient and intermediate layers comprise the transition zone of the upper permafrost; the transient layer forms as a result of interannual variations in the active-layer thickness (ALT), and the ice-rich intermediate layer forms as a result of a gradual decrease in the ALT, commonly caused by organic accumulation (Shur, 1988a, 1988b; Shur et al., 2005, 2011; French and Shur, 2010).

For the risk assessment, we consider the three protective layers (PL) of frozen soils above ice wedges (Fig. 4A): PL1 (total thickness of frozen soil above the ice wedge, which includes the frozen part of the active layer, transient layer, and intermediate layer); PL2 (includes transient and intermediate layers), and PL3 (intermediate layer). This color-coded system of risk evaluation (Fig. 4B) includes six risk levels, from bright red (risk level 1, the highest) to dark green (risk level 6, the lowest) (Kanevskiy et al., 2016). The two highest risk levels are related to currently degrading wedges. The difference between them is determined by the activity of degradation: while the first risk level refers to active degradation with significant thawing of ice wedges, the second level corresponds to slow degradation when the depth of seasonal thawing can reach the top surface of ice wedges only at the end of a warm season. The third risk level is related to ice wedges that are not currently degrading, but the protective layer is so thin that degradation can start very easily, and some parts of the studied wedges that belong to this category may already have undergone degradation at the time of this study.

4. Results

4.1. Soil, ground ice, and stable isotopes

Structure and properties of frozen soils and ground ice were studied at 113 boreholes up to 3.5 m deep at PB and at 54 boreholes up to 4.1 m deep at BW. Below we summarize soil stratigraphy within polygon centers that represent the main surficial deposits, ice-wedge dimensions and volume, the thickness of the protective layers formed by soils above the ice wedges, and stable isotopes concentrations in the ground ice. Characteristics are compared between study areas. Additionally, we compare the data on protective layer thicknesses from these areas with the data obtained from the 2.1-km-long CRREL transect (Fig. 1), where 80 boreholes ~1.0 m deep were drilled in spring 1963 (Brown and Johnson, 1965; Brown, 1969; Hinkel et al., 1996); thicknesses of protective layers above the ice wedges are estimated for this transect based on analysis of the photographs of frozen cores.

Soil stratigraphy and cryostructures in the centers of ice-wedge polygons at PB and BW were determined by detailed description of cores from three boreholes at each site (Figs. 5 and 6). At PB, the upper permafrost at these boreholes was composed mostly of organic-

A

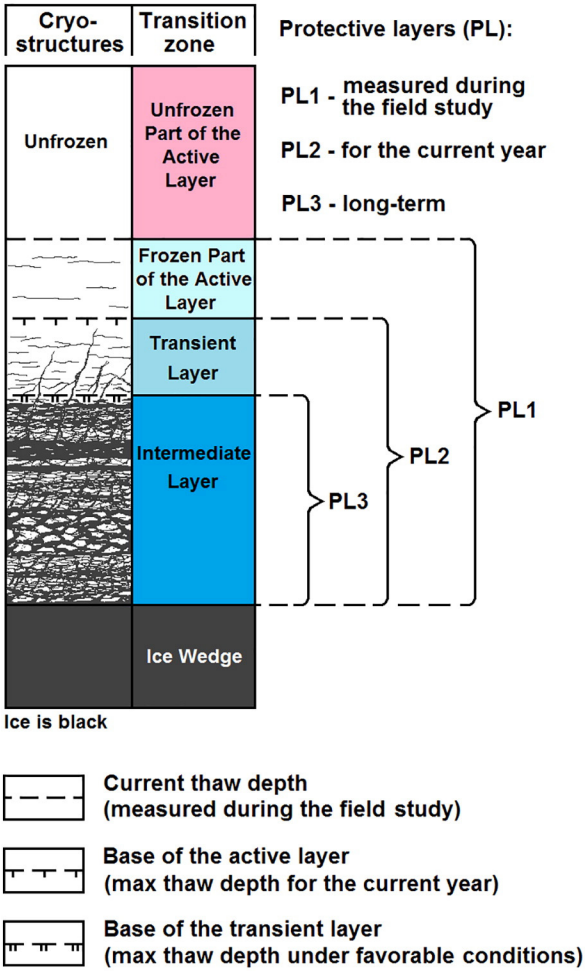

B

Risk level	Thickness of protective layers, cm			Notes
	PL1*	PL2**	PL3*	
1. Active degradation	0	0	0	No protective layers; the top part of the ice wedge is currently* degrading; degradation of the ice wedge of up to 5 cm is expected by the end of warm season
2. Very high	1-5	0	0	Degradation of the top part of the ice wedge is expected by the end of warm season
	=PL3	0	1-5	Thin intermediate layer is currently* degrading; degradation of the top part of the ice wedge is expected by the end of warm season
3. High	5-10	1-5	0	No intermediate layer, thin degrading transient layer; minor degradation of some parts of this ice wedge is possible by the end of warm season
	5-10	1-5	1-5	Partial degradation of the intermediate layer is expected by the end of warm season; minor degradation of some parts of this ice wedge is possible by the end of warm season
	=PL3	1-5	5-10	Intermediate layer is currently* degrading; minor degradation of some parts of this ice wedge is possible by the end of warm season
4. Moderate	10-20	5-15	1-5	No significant degradation of the intermediate layer and no ice-wedge degradation are expected during the current year
	10-20	5-15	5-10	Partial degradation of the intermediate layer is possible by the end of warm season; no ice-wedge degradation is expected during the current year
	=PL3	5-15	10-20	Relatively thick intermediate layer is currently* degrading; no ice-wedge degradation is expected during the current year
5. Low	20-30	15-25	5-10	No degradation of the intermediate layer is expected during the current year
	20-30	15-25	10-20	No significant degradation of the relatively thick intermediate layer is expected during the current year
	=PL3	>15	>20	Thick intermediate layer is currently* degrading
6. Very low	>30, >PL3	>25, >PL3	>20	The ice wedge is well protected by thick and stable intermediate layer; ice-wedge degradation is possible only due to a strong impact on the surface (flooding, vegetation removal) or after accumulation of wedge ice within the intermediate layer

* Measured from late July to mid-August
** Measured from late August to mid-September (PL1=PL2)

Fig. 4. Estimation of risk of ice-wedge degradation. (A) Protective layers of frozen soils preventing wedge ice from thawing; (B) evaluation of risk of the ice-wedge degradation for northern Alaska based on thicknesses of protective layers (modified from Kanevskiy et al., 2016).

mineral soils (organic silts with peat inclusions), which we interpret to be of lacustrine origin, ~2.5 m thick. Gravel inclusions were encountered from 1.3 m (borehole PB-HC3-256) and ~2.0 m (PB-HC1-156 and PB-HC2-80). Coarse mineral soils (gravelly sands with some peat inclusions) were encountered at ~2.5 m in boreholes PB-HC1-156 and PB-HC2-80. The most common cryostructures for organic silt and mineral soils were ataxitic and reticulate, with numerous horizontal ice layers (belts) up to 3 cm thick; organic-matrix cryostructure was observed in peat.

At BW, the upper permafrost in boreholes BW-HC1, BW-HC2, and BW-HC3 was composed mostly of silty sands with numerous peat layers and inclusions and occasional gravel inclusions. The most common cryostructures were ataxitic (in mineral soils) and organic-matrix (in peat). Age of studied deposits at BW varied from ~4300 (at 0.7 m) to 10,500 C_{14} y BP (at 3.8 m) in BW-HC3; similar dates were obtained in BW-HC1 (Fig. 6). Gravimetric (GMC) and volumetric (VMC) moisture contents of soils were determined for these boreholes (Figs. 5 and 6). At PB, average values for the permanently frozen soils were very high: GMC = 235.4% (n = 27), and VMC = 82.5% (n = 25). At BW, average values for the permanently frozen soils were slightly lower: GMC = 141.0%, and VMC = 78.4% (n = 39).

Massive ground ice (wedge ice and thermokarst-cave ice) was encountered in 83 of 113 (73.4%) boreholes at PB (Table S1) and in 44 of 54 (81.5%) boreholes at BW (Table S2). At the CRREL transect near Barrow, ice wedges were encountered in 22 of 80 (27.5%) boreholes (Table S3), but if we exclude plots 14 to 25 (with elevations <2.5 m and rare ice wedges), this value increases to 37.5% (21 boreholes of 56). At PB, profiles across and along ice-wedge troughs (Figs. 7, S2, and S3)

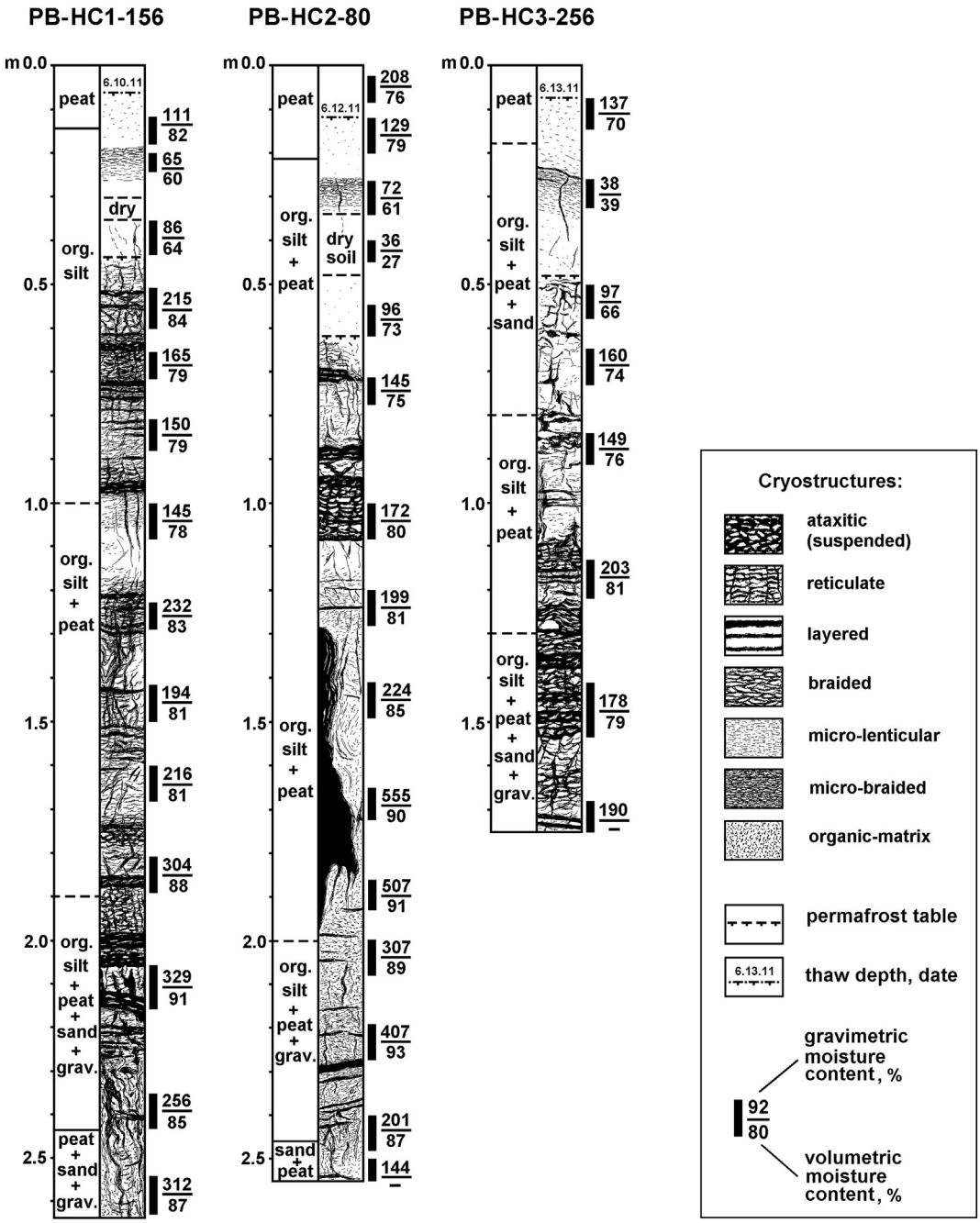

Fig. 5. Cryostratigraphy and moisture contents of the active layer and upper permafrost, Prudhoe Bay study area (for locations, see Fig. 2).

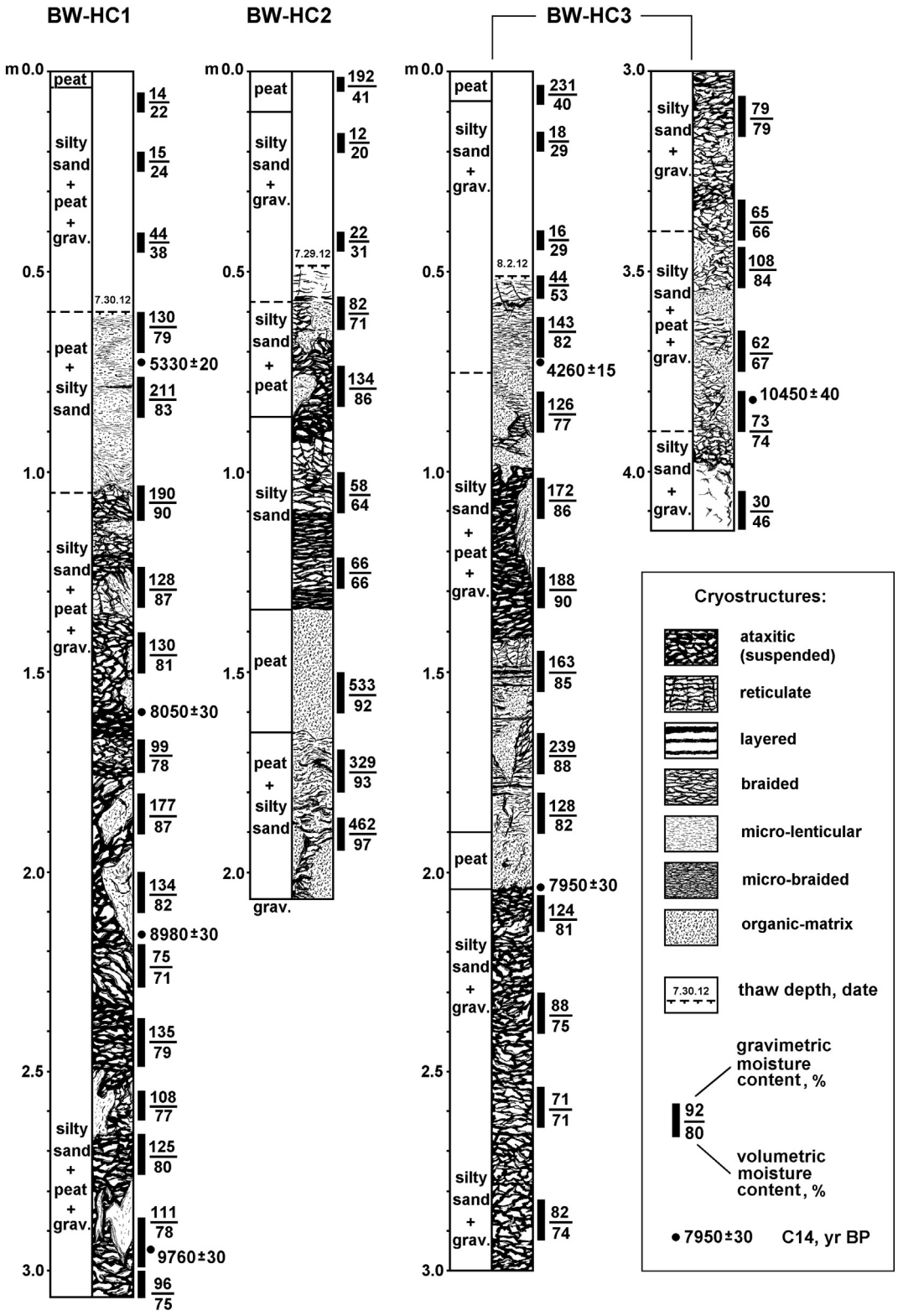

Fig. 6. Cryostratigraphy and moisture contents of the active layer and upper permafrost, Barrow study area (for locations, see Fig. 3).

reveal that a width of wedges varied from 1.5 to 3.5 m, and their vertical extent was ~3 m. At BW, profiles across ice-wedge troughs are shown in Figs. 8, S4; width of ice wedges in this area varied from 2 to 9 m. At PB, mean ice wedge volume in the upper 3 m of permafrost (as % of layer volume) was 21.5 ± 6.3% (±SD), calculated from their average cumulative length of 1406 ± 39 m/ha determined from air photos and a cross-sectional area of 5.1 ± 1.5 m^2 determined from coring five wedges (Jorgenson et al., 2015). At BW, mean ice-wedge volume in the upper permafrost was ~36% (calculated according to Kanevskiy et al., 2013), assuming that the average ice-wedge width was ~5 m ($n = 4$, see Fig. 8), and the average size of polygons was ~12 m ($n = 10$, Fig. 3). Thermokarst-cave ice occurred in 26.5% and 13.0% of

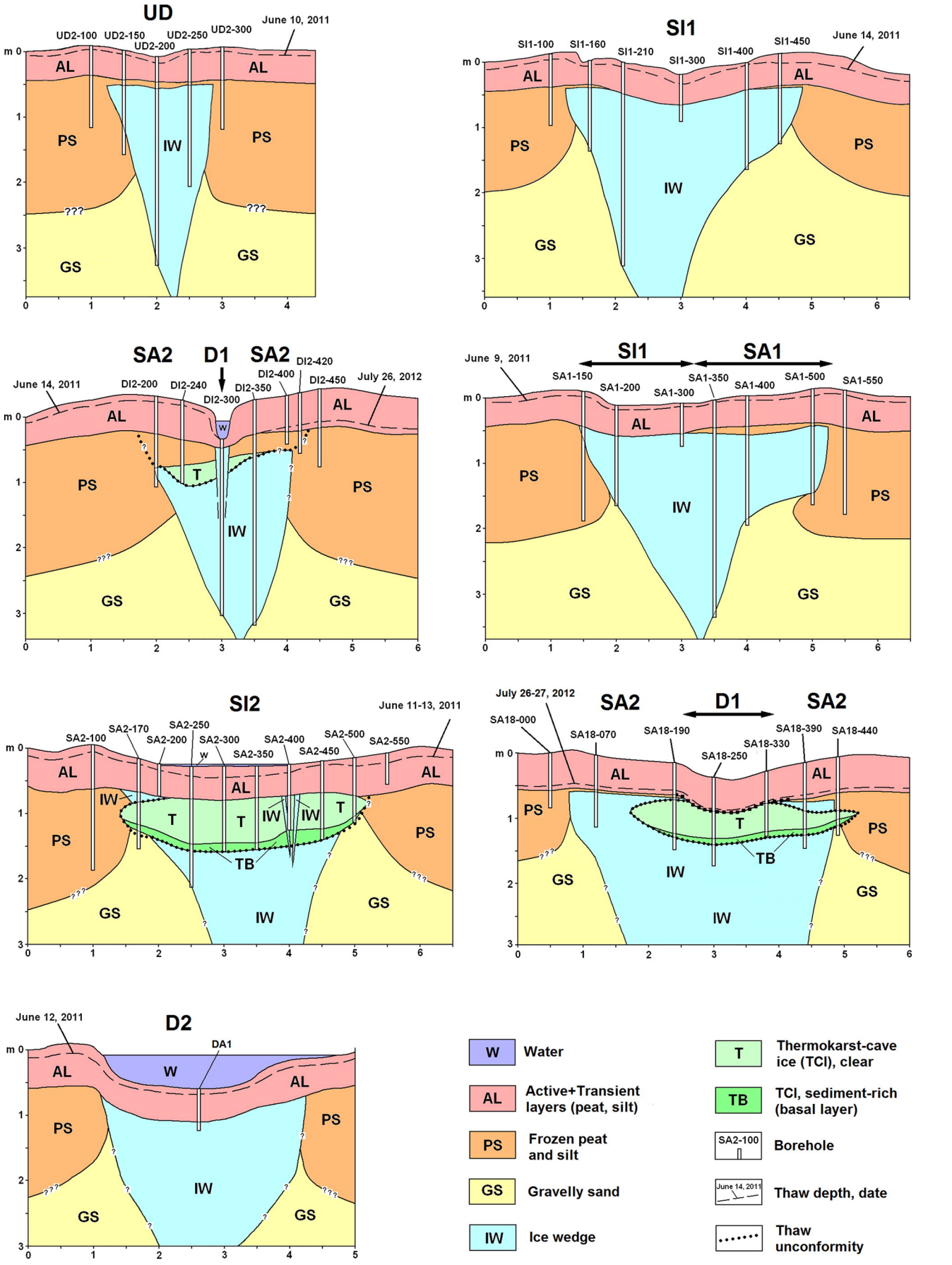

Fig. 7. Cross sections of ice wedges, Prudhoe Bay study area (for location of profiles, see Figs. 2 and S2) (modified from Jorgenson et al., 2015). Stages of ice-wedge degradation/stabilization are labeled according to Fig. 12, Table 1.

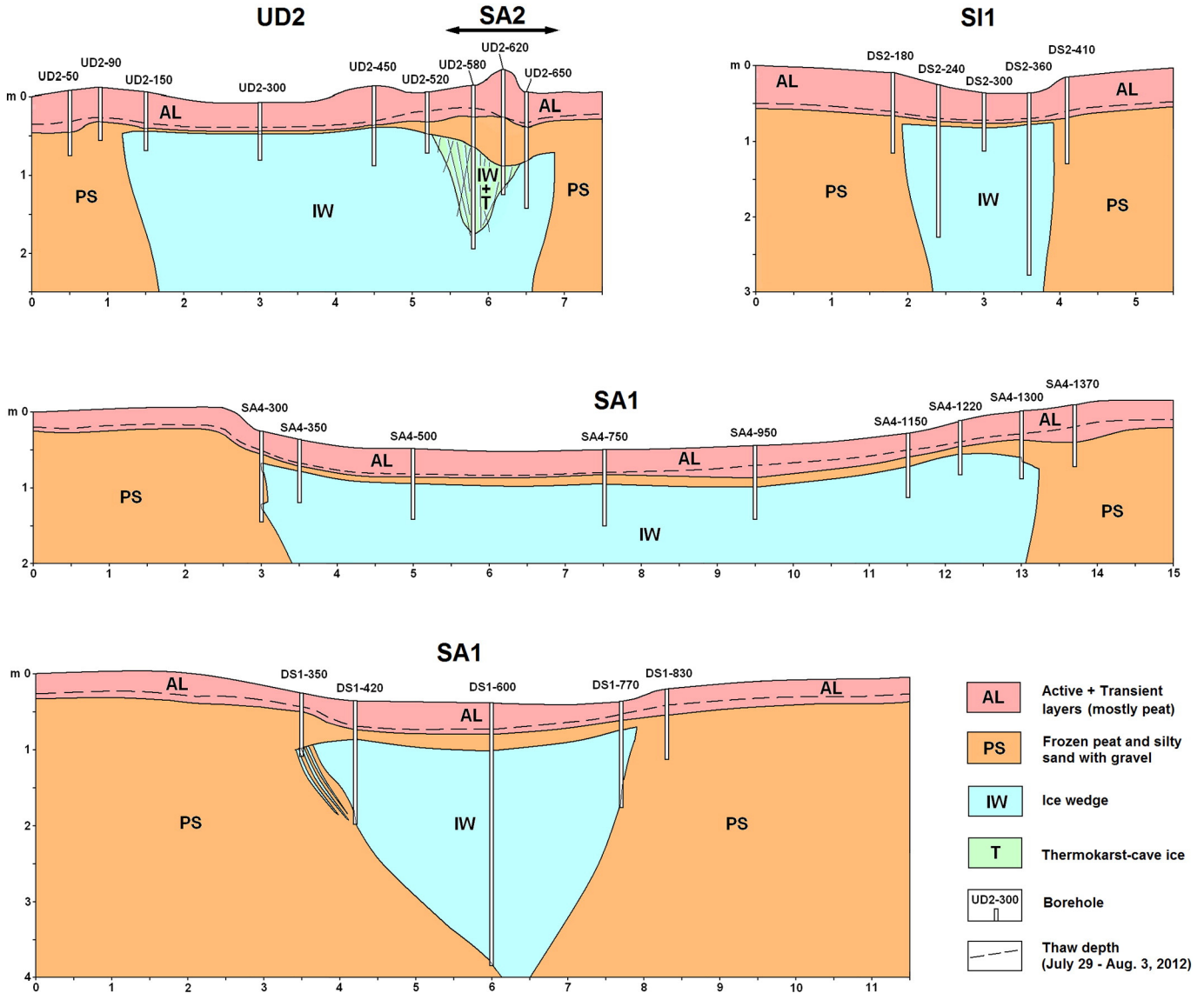

Fig. 8. Cross sections of ice wedges, Barrow study area (for location of profiles, see Figs. 3 and S3). Stages of ice-wedge degradation/stabilization are labeled according to Fig. 12, Table 1.

boreholes at PB and BW respectively (Tables S1 and S2); it was more often encountered at SI and SA sites (within or adjacent to ice wedges at various stages of stabilization).

In many cases, massive-ice bodies were protected by the frozen intermediate layer (IL) of the upper permafrost, up to 84 (PB), 70 (BW), and 36 cm (CRREL transect) thick, with an average thickness of 8.6 (PB), 13.3 (BW), and 6.6 cm (CRREL transect) (Tables S1, S2, and S3). The IL tended to be thinner at PB (<1 cm in >45% of boreholes), compared to BW (Fig. 9), where thickness intervals of 2–5, 6 − 10, and 11 − 20 cm were more common (>20% each), and IL <1 cm thick was encountered in only 11% of boreholes. At the CRREL transect near Barrow, IL <1 cm thick was detected in the 1963 photographs in ~41% of boreholes, and a thickness interval of 11 − 20 cm was also common (~27%).

Stable isotopic composition of ground ice and surface water was analyzed for 47 samples collected from PB and 22 from BW (Table S4, Fig. 10). Most of the samples were obtained from ice wedges ($n = 38$) and thermokarst-cave ice ($n = 12$), with fewer samples from thermokarst-cave ice dissected by ice veins ($n = 6$), segregated ice ($n = 6$), and water from thermokarst troughs ($n = 7$). Mean values of $\delta^{18}O$ isotope for ice wedges were $-23.4 \pm 2.1‰$ for PB ($n = 23$) and $-21.3 \pm 1.4‰$ for BW ($n = 15$). Mean $\delta^{18}O$ values for thermokarst-cave ice were $-19.1 \pm 2.5‰$ for PB ($n = 11$) and $-18.1 \pm 1.7‰$ for BW ($n = 2$). Mean $\delta^{18}O$ value for thermokarst-cave ice dissected by ice veins was $-20.3 \pm 3.7‰$ at PB ($n = 6$); these values look reasonable for samples that contain wedge and thermokarst-cave ice. Mean $\delta^{18}O$ values for segregated ice were $-15.9 \pm 2.6‰$ for PB ($n = 4$) and $-15.8‰$ for BW ($n = 1$). Mean $\delta^{18}O$ values of standing water from the ice-wedge troughs were much lower at PB ($-16.0 \pm 0.9‰$, $n = 3$, sampled in June) than in BW ($-10.1 \pm 4.5‰$, $n = 4$, sampled in August). While for sites BW-DA1, −DA2, and -DA3 the $\delta^{18}O$ values of standing water varied from -7.0 to $-8.7‰$, the value for BW-DA6 was $-16.8‰$ (Table S4).

4.2. Environmental factors

Environmental factors that affect the degradation of ice wedges are those that control the thickness of the active layer. They include air temperature, precipitation, ground temperature, microtopography, water depth, snow thickness, and vegetation.

At PB, annual mean air temperature measured at our transect at 1.5 m aboveground during the 2012 hydrologic year (September 2011 to August 2012) was −10.6 °C (Jorgenson et al., 2015). Climatic data from NOAA summarized for the 1981 − 2010 period (Alaska Climate

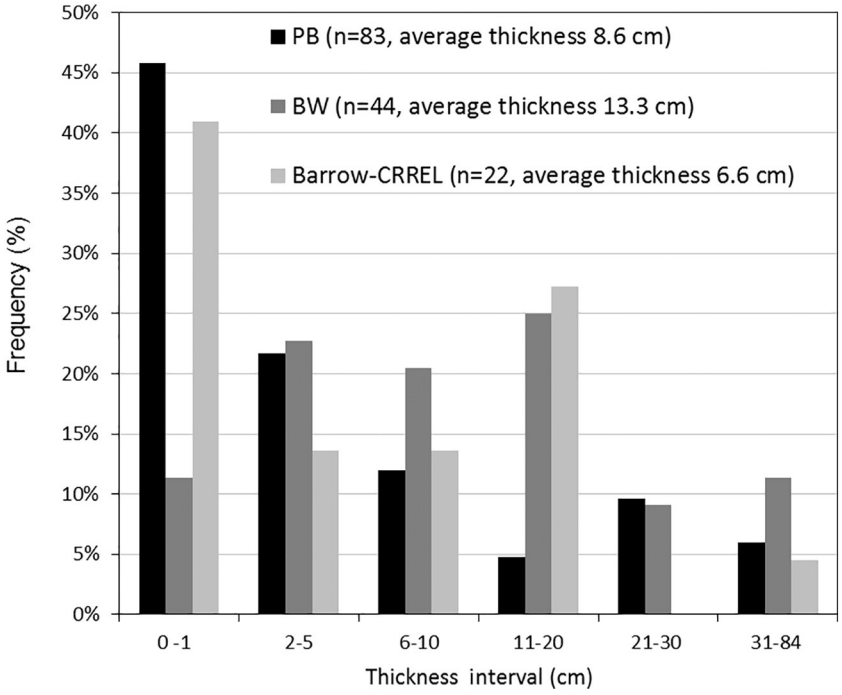

Fig. 9. Occurrence of differing thickness intervals of the intermediate layer across all cores that encountered massive-ice bodies (wedge ice and/or TCI), Prudhoe Bay (PB – 2011, 2012) and Barrow (BW – 2012, CRREL – 1963) study areas in northern Alaska.

Research Center, http://climate.gi.alaska.edu/Climate/Normals) show that mean annual air temperature (MAAT) at Prudhoe Bay was −11.1 °C, annual precipitation 102.6 mm, and annual snowfall 85.6 cm. At Barrow, MAAT was −11.2 °C, annual precipitation 115.1 mm, and annual snowfall 95.8 cm. Though MAAT at Prudhoe Bay and Barrow were almost equal, significant seasonal differences in air temperatures existed between these areas. Freezing index atBarrow, averaged for the 1981−2010 period, was −4424.0 °C-day, while thawing index was 335.8 °C-day. At Prudhoe Bay, these indexes were −4637.6 °C-day and 593.3 °C-day, correspondingly, which indicates warmer summers and somewhat colder winters in comparison with Barrow.

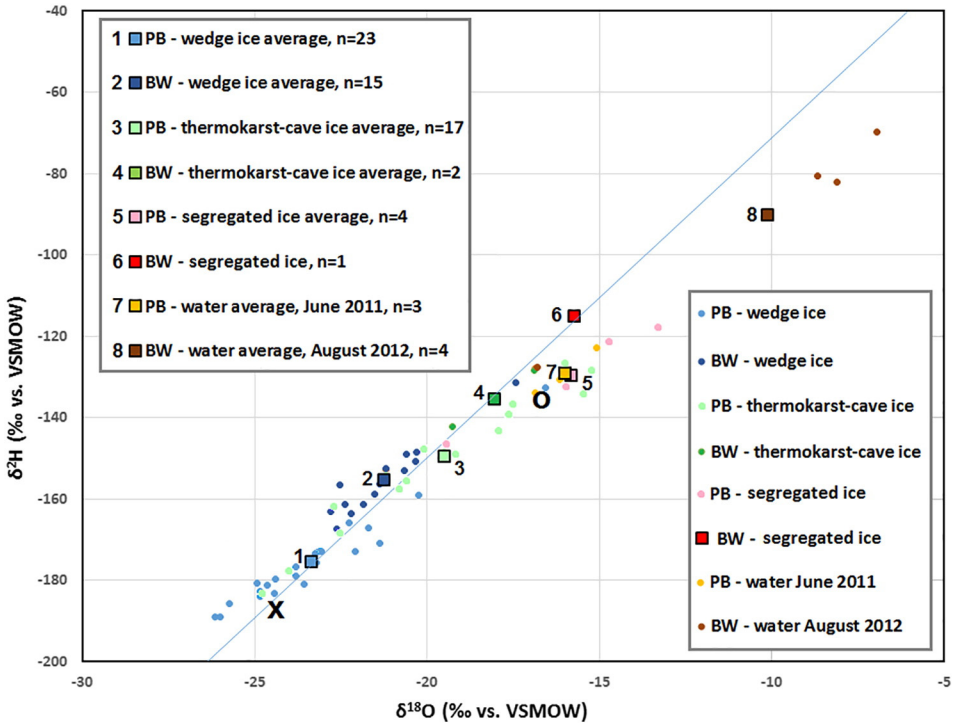

Fig. 10. $\delta^{18}O$–$\delta^{2}H$ diagram for different types of ground ice and surface water in PB and BW study areas. Blue line represents the Global Meteoric Water Line (GMWL). Average values for buried ice wedges ($n = 121$) and segregated ice ($n = 15$) obtained from the Buried Ice-Wedge Tunnel in Barrow (Meyer et al., 2010) are marked with X and O, correspondingly.

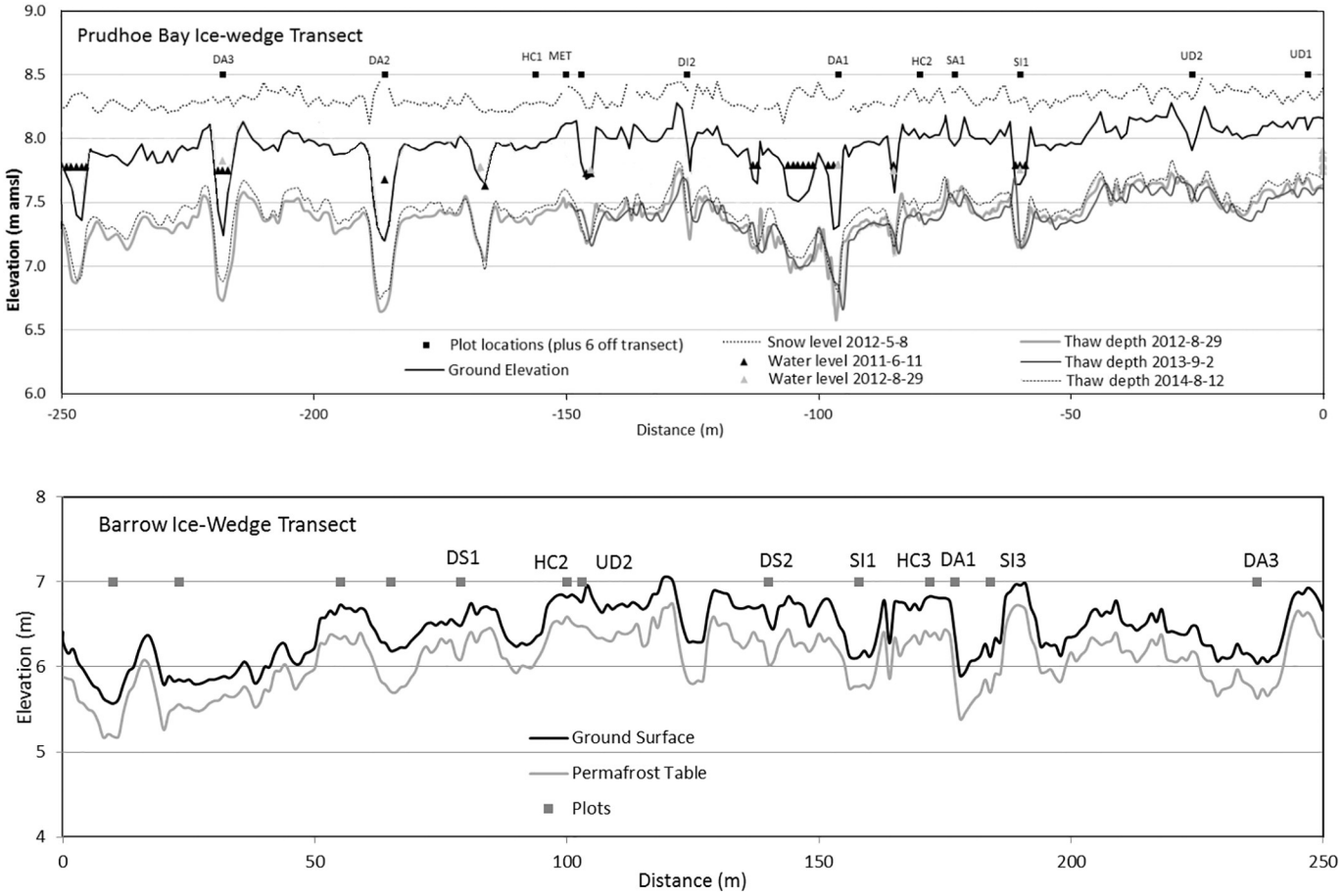

Fig. 11. Cross sections of the sampling transects. Top – Prudhoe Bay, PB study area, June 2011–August 2014 (based upon Jorgenson et al., 2015); bottom – Barrow, BW study area, early August 2012.

At PB, annual mean surface temperatures measured along the transect during 2012 varied significantly among degradation/stabilization stages: from −6.2 °C (UD) to −1.3 °C (DA). Annual mean ground temperature measured at 50 cm below the surface (near the permafrost table) had similar trends, ranging from −7.3 °C (UD) to −3.5 °C (DA) (Jorgenson et al., 2015). In the adjacent area (Deadhorse site, N70.161283 W148.4653), mean annual ground temperature (MAGT) measured at 20-m depth had increased during the last decades from −8.7 °C (1978) to −5.6 °C (2015); more rapid increase in MAGT started in 1993 (Romanovsky et al., 2016). The MAGT at the Barrow site (N71.309033 W156.661517) measured at the 20-m depth had increased from −9.1 °C (2003) to −8.5 °C (2015) (Romanovsky et al., 2016).

Measurements of seasonal thaw were performed every 1 m along the 250-m PB transect several times in 2012–2015 (Table S5). These measurements revealed relatively small interannual differences in the ALT: mean thaw depth was 56.2 cm on 29 August 2012, 59.0 cm on 2 September 2013, and 58.7 cm on 16 September 2015. Increase in thaw depth measured between 7 August and 16 September 2015 was <2 cm, but measurements performed in 2012 revealed a very significant (almost 13 cm) increase in thaw depth between 26 July and 29 August. Comparison of average thaw depths measured on 11 August 2014 and 7 August 2015 showed that in 2014 (very cold summer) thaw depth was ~7 cm (~12%) shallower than in 2015 (Table S5). At BW, thaw depths along the 250-m transect were measured only once (29 July 2012), and the mean thaw depth value at that time was 35.3 cm. At the CRREL transect near Barrow, the mean ALT values in 1962–2014 varied from 23 to 40 cm; in 2012, it was 38 cm (Brown et al., 2015). According to this study, maximum summer thaw in Barrow generally occurs by mid-August.

Similarly to air and ground temperatures, active-layer thicknesses also varied among stages. At PB, mean thaw depths in late July 2012 were significantly lower in UD (43.5 cm) and DI (39.7 cm) compared to DA (52.3 cm), SI (46.4 cm), SA (51.6 cm), and polygon centers (59.0 cm); similarly, mean snow depths were much deeper in DA (52.2 cm) compared to UD (31.8 cm) (Jorgenson et al., 2015). At BW, mean thaw depths in late July – early August 2012 in UD (32.7 cm) and SA (32.5 cm) were significantly lower than in DA (50.3 cm); values for DI and SI stages were intermediate (~40 cm).

Microtopography at PB and BW is characterized by abundant thermokarst troughs over degrading ice wedges (Fig. 11). At PB, the maximum depths of the larger troughs associated with DA stage tended to be 0.5 to 0.9 m below the adjacent polygon centers (water depths varied from 0.3 to 0.5 m), the widths of these troughs at the top tended to be 1 to 4 m, and the tops of the polygons tended to be 8 to 15 m across. At BW, the maximum depths of the larger troughs associated with DA tended to be 0.8 to 1.1 m below the adjacent polygon centers, the widths of troughs at the top tended to be 3 to 8 m, and the polygon centers tended to be 6 to 12 m across.

Surface water was commonly impounded in thermokarst troughs and pits as indicated by the topographic profiles for PB and BW (Fig. 11). At PB, mapping of surface water found that water covered 7.5% of the study area in 2012 (Figs. 2, S18, and S20). Jorgenson et al. (2015) delineated thermokarst troughs around the PB transect using aerial photos (time series of eight images from 1949 to 2012) and found that the area occupied by water-filled troughs increased from

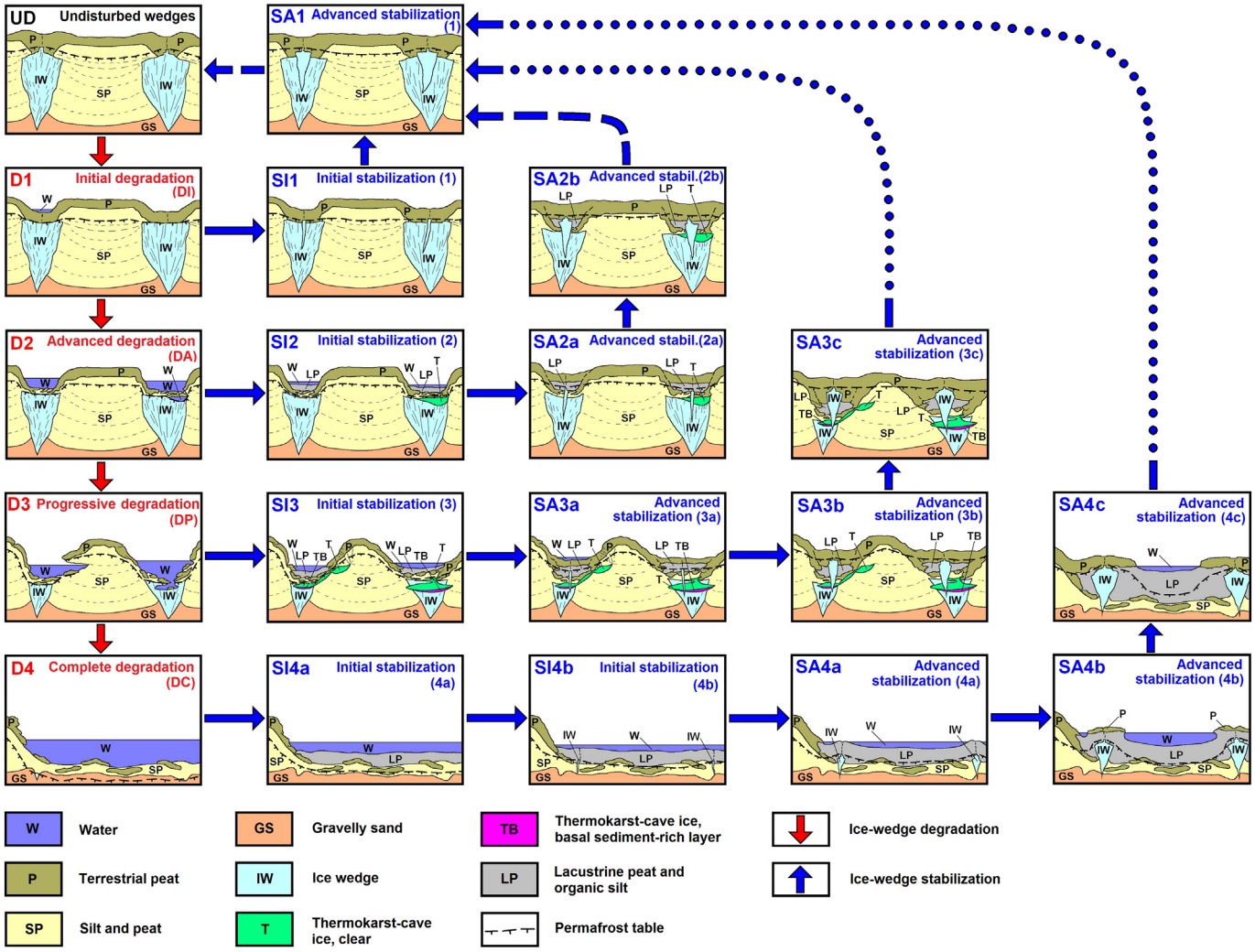

Fig. 12. Stages of ice-wedge degradation and stabilization.

0.9 to 1.5% in 1949–1988 and from 1.5 to 7.5% in 1988–2012 (Figs. S18 and S20). They attributed the recent ice-wedge degradation to extremely warm and wet summers in 1989 and 1998. As a result of ice-wedge degradation, many of the low-centered polygons visible on 1949 aerial photos have transformed into high-centered or transitional (from low- to high-centered) ice-wedge polygons; the latter are characterized by deep troughs surrounded by elevated rims. Similar trends were detected at the adjacent Colleen site A, located ~2 km southwest of our transect within the same lake basin; this site was strongly affected by road construction and heavy traffic along Spine Road (Walker et al., 2014, 2015; Buchhorn et al., 2016; Kanevskiy et al., 2016). Widespread degradation of ice wedges has been observed for decades in the larger area of the Prudhoe Bay Oilfield (Raynolds et al., 2014).

Surface water covered only 1.2% of the BW study area in 2014 (Figs. 3, S19, and S20). Unlike PB, this area is characterized by high-centered polygons, which formed as a result of large-scale ice-wedge degradation that happened many decades ago. Analysis of aerial photos shows that since 1948 processes of ice-wedge degradation/stabilization have affected various parts of this area but have not changed the type of terrain: relatively well drained high-centered polygons with deep troughs existed in 1948 and in 2014, when randomly distributed water bodies occupied 2.8 and 1.2% correspondingly. The last cycle of degradation/stabilization occurred at BW in the 1950s–2000s; during this cycle, the area of water-filled troughs reached 13% in 1955 and stayed at the very high level until the late 1990s with a following decrease from 12.8 to 1.4% in 1997–2005 (Figs. S19 and S20).

Vegetation composition varied widely among stages at PB and BW. At PB (Jorgenson et al., 2015), vegetation was similar for central parts of high-centered polygons (HC) and UD sites, where dwarf shrubs (*Dryas integrifolia*, *Salix arctica*, and *Salix richardsonii*) were abundant. The DI stage was dominated by sedges (*Eriophorum angustifolium* and *Carex bigelowii*). By the DA stage, a large shift to the aquatic calcareous mosses (*Calliergon giganteum* and *Scorpidium scorpioides*) and aquatic forbs (*Utricularia vulgaris* and *Hippuris vulgaris*) occurred. At the SI stage, aquatic sedges (*Carex aquatilis* and *E. angustifolium*) dominated. The SA stage had abundant dwarf shrubs similar to UD, but differed from the latter by the abundance of the sedge *Carex membranacea*. At BW, the HC sites were dominated by dwarf shrubs (*Salix pulchra*, *S. rotundifolia*), graminoids (*Luzula confusa*, *Poa arctica*), and lichens (*Dactylina arctica*, *Thamnolia vermicularis*); whereas UD was dominated by graminoids (*Arctagrostis latifolia*, *Poa arctica*, *Eriophorum scheuchzeri*, *Carex aquatilis*) and mosses (*Dicranum elongatum*, *Sphagnum fimbriatum*). The DI stage was dominated by grasses (*Alopecurus alpinus*, *Poa arctica*), sedges (*Carex aquatilis*, *Luzula confusa*), and *Sphagnum* mosses. The DA stage was dominated by aquatic graminoids (*Arctophila fulva*, *C. aquatilis*, *Dupontia fisheri*) and mosses (*Calliergon richardsonii*, *C. giganteum*). The SI stage was dominated by aquatic graminoids (*C. aquatilis*, *Eriophorum scheuchzeri*, *D. fisheri*) and more abundant mosses (*Calliergon richardsonii*,

Warnstorfia exannulata, *Sphagnum squarrosum*). By the SA stage, the dominant species were similar, but a diversity of species was much higher. We attribute the large difference in species between PB and BW to PB having carbonate-rich soils and BW having acidic soils.

4.3. Stages of ice-wedge degradation and stabilization

Based on our field data and observation, we modified previous conceptual models depicting stages of ice-wedge degradation and stabilization (Jorgenson et al., 2006, 2015; Raynolds et al., 2014). The following charts (Fig. 12) reflect our contemporary understanding of these processes. Characteristics of the main stages of the ice-wedge degradation and stabilization are presented in Table 1, based in part on the quantitative characteristics of sites (Tables S1 and S2) and descriptions of vegetation. Within our PB and BW study areas, we could detect most of the stages except SI3, SI4, SA3, and SA4. Thus, these four stages were presented in Fig. 12 and Table 1 based not on real data but on our general comprehension of degradation/stabilization processes.

Typically, *undisturbed ice wedges* (*UD*) are mostly active (currently growing) and protected by a well-developed intermediate layer (Tables S1 and S2). Usually these wedges form low-centered or flat-centered ice-wedge polygons. Typical cross sections of undisturbed ice wedges are shown in Fig. 7 (PB, profile UD2), and Fig. 8 (BW, profile UD2); photographs of the individual cores are shown in Fig. S5.

The *initial degradation stage* (*D1*), which corresponds to DI (Jorgenson et al., 2006, 2015), is characterized by complete degradation of the original intermediate layer with formation of shallow thermokarst troughs, which are mostly dry or periodically filled with shallow water. We presume that during this stage the formation of ice wedges is not interrupted, and despite a partial degradation of ice wedges from the top, lateral growth of wedges continues. Cross sections across the troughs above the actively degrading wedges (D1 stage) at PB are shown in Fig. 7 (borehole DI2-300 in the profile DI2, central part of the profile SA18); photographs of the individual cores are shown in Fig. S6. This stage can be easily reversed to SI1 (and then to SA1); in many cases, such transitions can be difficult to detect. When the IL thickness is very small, further transformations of the ice wedge can go both ways –– to degradation or stabilization, depending on climate fluctuations or vegetation succession.

The *advanced degradation stage* (*D2*), which corresponds to DA (Jorgenson et al., 2006, 2015), is characterized by active melting of ice wedges and formation of large troughs filled with water (or ice in the winter). The intermediate layer is totally degraded. Cross sections across the troughs above the actively degrading wedge (D2 stage) at PB are shown in Fig. 7 (profile DA1); photographs of the individual cores are shown in Fig. S7.

During the *progressive degradation stage* (*D3*), deep degradation of ice wedges occurs with formation of large and deep ponds connected with underground cavities whose development was triggered either by running or standing water; large niches can form as a result of expansion of deep ponds beyond the ice wedge boundaries. This stage is not common for our study areas, and we have detected it only once (BW, site DA6, Figs. S12–S16). In most cases, ice-wedge degradation terminates at stages D1 or D2.

Further development of deep thermokarst ponds potentially leads to *complete degradation* (*D4*) of ice wedges that affects the central parts of polygons as well. As a result, initial ponds can transform into larger thaw lakes. While truncated ice wedges can still exist under shallow lakes, an increase in water depth eventually leads to talik formation and complete degradation of ice wedges. Further expansion of large thaw lakes occurs mainly through formation of thermoerosional niches caused by wave activity but may be prevented by the lake drainage, which leads to refreezing of the talik. We presume that under current climatic conditions transformation from D3 to D4 occurs very seldom. We have not detected stage D4 at our study sites, but old thermokarst ponds in the adjacent areas (e.g., large ponds visible in Fig. 2) probably represent this stage.

The *initial stabilization stage* (*SI1*) *for wedges slightly degraded during stage D1* is characterized by shallow, relatively dry troughs. It starts with IL recovery accompanied by further development of ice wedges. Transitions between SI1 and D1 are easily reversible, and drilling is required to distinguish this stage from D1. Cross sections across the wedges at the stage of initial stabilization SI1 for PB and BW are shown in Fig. 7 (profile SI1, part of profile SA1) and Fig. 8 (profile DS2), correspondingly; photographs of the individual cores are shown in Fig. S8.

The *initial stabilization stage* (*SI2*) *for wedges that have degraded during stage D2* starts with IL recovery and/or TCI bodies formation under the water-filled troughs. It is triggered by either organic accumulation or by drainage of thermokarst ponds. Cross sections across the wedges at the stage of initial stabilization SI2 for PB are shown in Figs. 7 (profile SA2) and **S3**; photographs of the individual cores are shown in Fig. S9.

The *initial stabilization stage* (*SI3*) *for wedges that have degraded during stage D3* is usually triggered by partial drainage of deep troughs and ponds. At this stage, residual shallow ponds still occur in deep troughs. During this stage, the IL recovery begins, but ice-wedge formation is not very active.

The *initial stabilization stage* (*SI4*) *after complete degradation of ice wedges* (*stage D4*) includes two substages (Fig. 12). *Substage SI4a* starts with partial drainage of the thaw lake and freezing of the talik. *Substage SI4b* includes further decrease in water depth, continuing accumulation of lacustrine sediments with formation of syngenetic permafrost, and initial subaquatic development of thin ice wedges.

The *advanced stabilization stage* (*SA1*) *for wedges slightly degraded during stage D1* is characterized by recovery of IL and continuing development of existing ice wedges, and it is difficult to distinguish this stage from UD. Cross sections across the wedges at stage SA1 for PB and BW are shown in Fig. 7 (right part of profile SA1) and Fig. 8 (profiles DS1 and SA4), correspondingly; photographs of the individual cores are shown in Fig. S10.

The *advanced stabilization stage* (*SA2*) *for wedges*, *which have degraded during stage D2* is characterized by draining of troughs, further accumulation of organic matter in troughs, active development of the IL, whose thickness usually exceeds that of UD, and formation of ice wedges that penetrate into older ice wedges previously affected by degradation. Cross sections across the wedges at stage SA2 for PB and BW are shown in Fig. 7 (profiles DI2, SA18) and Fig. 8 (right part of profile UD2), correspondingly; photographs of the individual cores are shown in Fig. S11.

The *advanced stabilization stage* (*SA3*) *for wedges that have degraded during stage D3* includes three substages (Fig. 12). *Substage SA3a* is characterized by wet troughs with shallow water, further development of the IL, and active formation of young ice wedges within the IL and/or large TCI bodies; these wedges can penetrate into old degraded ice wedges. *Substage SA3b* is characterized by draining of troughs, decrease in the ALT and depth of troughs caused by moss accumulation, and further development of the IL and ice wedges. *Substage SA3c* is characterized by filling troughs with organic soils and widening of ice wedges.

The *advanced stabilization stage* (*SA4*) *for wedges that have completely degraded during stage D4* includes three substages (Fig. 12). *Substage SA4a* is characterized by further development of new ice wedges with emergence of ridges above the water level. *Substage SA4b* is characterized by formation of low-centered polygons with well-developed ridges and deep intrapolygonal ponds, accumulation of terrestrial peat, and decrease in the ALT within elevated ridges. *Substage SA4c* is characterized by widening of ice wedges, accumulation of organic soils, and decrease in water depth in intrapolygonal ponds that eventually leads to decrease in the ALT, permafrost aggradation and frost heave of organic soils, and vanishing of ponds.

The occurrence of TCI bodies (Fig. S17) depends on the depth of ice-wedge degradation and is common at SI2, SI3, SA2, and SA3 stages

Table 1
Main stages of ice-wedge degradation and stabilization and their characteristics (see Fig. 12).

Stage	Duration, years	Water, cm	Ice wedges (IW)	Intermediate layer (IL), average thickness, cm	Thermokarst-cave ice (TCI)	Vegetation
UD – undisturbed ice wedges	Variable	0	Undisturbed ice wedges	Undisturbed PB: 8.6 ($n = 9$) BW: 7.2 ($n = 9$)	Relict TCI bodies occasionally occur (formed during previous degradation events)	Dwarf shrubs (PB) Graminoids and mosses (BW)
D1 – initial degradation	<10	<10	Ice wedges melt with thaw subsidence up to 20–30 cm; wedges continue growing laterally	Total degradation PB: 0.8 ($n = 10$) BW: 0.0 (n = 1)	Partial degradation of relict TCI bodies	Dwarf shrubs, sedges (PB) Grasses, sedges, sphagnum(BW)
D2 – advanced degradation)	<10–10s	10s	Degradation with thaw subsidence up to 100 cm	Total degradation PB: 0.5 ($n = 4$) BW: 0.0 ($n = 3$)	Small cavities on top of ice wedges filled with water; partial or total degradation of relict TCI bodies	Calcareous aquatic mosses, forbs (PB) Aquatic graminoids and mosses (BW)
D3 – progressive degradation	<10–10s	10s–100	Degradation with thaw subsidence up to 200 cm	Total degradation	Cavities filled with water may form deep niches outside the boundaries of IW; total degradation of relict TCI bodies	Calcareous aquatic mosses, forbs (PB) Aquatic graminoids and mosses (BW)
D4 – complete degradation	10s–100s	100s	Total degradation with thaw subsidence of >300 cm, which affects the central parts of polygons as well	Total degradation	Total degradation of relict TCI bodies	No vegetation
SI1– initial stabilization	<10	0	Wedges continue growing laterally	Initial recovery PB: 0.8 ($n = 16$) BW: 5.8 (n = 4)	Relict TCI bodies occasionally occur (formed during a previous degradation cycle)	Dwarf shrubs, sedges (PB) Grasses, sedges, sphagnum (BW)
SI2 – initial stabilization	<10–10s	0 to 10s	Formation of IW is possible if the water depth is <20–30 cm	Initial recovery PB: 0.0 ($n = 8$) BW: 6.7 ($n = 6$)	Relatively small TCI bodies may form	Aquatic sedges (PB) Aquatic graminoids and mosses (BW)
SI3 – initial stabilization	10 s	<10 to 10s	Formation of IW is not active but possible if the water depth is <20–30 cm	Initial recovery	Formation of TCI bodies is common	Aquatic sedges (PB) Aquatic graminoids and mosses (BW)
SI4 – initial stabilization	10s–100s	<10 to 10s	Initial sub-aquatic IW formation	Totally degraded	No TCI bodies can form	Not recorded: likely *Arctophila fulva*, *Carex aquatilis*
SA1 – advanced stabilization	<10–10s	0	Wedges continue growing laterally and vertically (in the recovering intermediate layer)	Recovery PB: 5.6 (n = 8) BW: 16.5 (n = 12)	Relict TCI bodies occasionally occur (formed during a previous degradation cycle)	Dwarf shrubs, sedges (PB) Graminoids and mosses (BW)
SA2 – advanced stabilization	10s–100s	0	Formation of young IW within IL and/or TCI	Recovery PB: 20.3 ($n = 28$) BW: 29.4 (n = 9)	Preservation of TCI bodies under the developing IL	Sedges (PB) Aquatic graminoids and mosses (BW)
SA3 – advanced stabilization	100s	0	Formation of young IW within IL and/or TCI	Recovery	Preservation of TCI bodies under the developing IL	Not recorded: likely similar to SA2
SA4 – advanced stabilization	1000s	0	Sub-aquatic IW formation transforms into sub-aerial	Formation of the IL along with the rise of the permafrost table	No TCI bodies can form	Not recorded: likely similar to SA2

(Fig. 12, Table 1). We do not have a clear explanation of the formation of TCI bodies located right below the permafrost table, which were frequently encountered during our study at the PB area (Figs. 7, S3). We presume that some of these bodies could form in underground thermoerosional cavities developed inside eroded ice wedges at significant depth, and their present-day location right below the permafrost table may be related to subsequent thermokarst, which has affected the top parts of ice wedges after TCI formation. Otherwise, the water-filled cavities could originally form at the permafrost table as a result of thermokarst or thermal erosion, but the upper soil (the AL) in some places was protected from collapse by the vegetation mat. Further vegetation growth and soil accumulation on the surface resulted in permanent freezing of these shallow water bodies.

Identification of stages of ice-wedge degradation/stabilization during the field studies may be confused by occurrence of secondary ice wedges developing in the intermediate layer. Our experience shows that in two adjacent boreholes the thicknesses of the IL above the ice wedge can be completely different because one of them may encounter a new generation wedge, while another may miss it and encounter only the old wedge. Thus, only drilling of numerous boreholes across the same ice wedge can solve this problem. For example, in the borehole SA2 (PB study area, Table S1) the IL thickness was 84 cm, while no IL was detected in the adjacent SA2-B borehole, which was located in the same ice-wedge trough. In the BW study area (Table S3), the IL thickness in the borehole SA3 was 70 cm, while in the adjacent SA3-main borehole it was only 2 cm. Similarly, a secondary ice wedge in the IL was detected in profile DI2 (PB study area); this thin ice wedge experienced degradation, which did not affect the primary wedge protected by the IL (Fig. 7, note a narrow water-filled trough on top of the secondary wedge). Evidence of secondary ice-wedge formation inside the TCI bodies were detected in profiles SA2 and DI2 (PB study area, Fig. 7) and UD2 (BW study area, Fig. 8).

The estimated duration of different stages of the ice-wedge degradation and stabilization process (Table 1, second column) cannot be precise. Under certain conditions, transition from UD (or D1) to D3 may happen very fast. For example, our study of the development of the large pond with the deep thermoerosional niche (BW study area, site DA6, Figs. S12–S16) revealed that this pond did not exist in 2010 (see GoogleEarth image from 20 July 2010 in Fig. S16), while in August 2012 it was already ~3 m wide (Figs. S12, S14), and by September 2015 its width reached almost 6 m (Figs. S13, S15); note that photographs in Figs. S12 (top)/S13 and S14/S15 were taken from approximately the same vantage points. In August 2012, the actively developing thermoerosional niche was 170 to 220 cm deep (Fig. S12). In September 2015, no thermoerosional niche or exposed permafrost could be observed, and the pond looked relatively stable. We cannot explain what triggered such fast pond development, but we can speculate that it started when the ice-rich permafrost was exposed by thermal erosion.

4.4. Evaluation of risk of ice-wedge degradation

Evaluation of the risk of ice-wedge degradation requires information on the thickness and properties of soil layers overlaying and protecting ice wedges (Fig. 4A). Especially important is the information on thickness of the intermediate layer (PL3), which facilitates the long-term stability of ice wedges. According to the color-coded system of risk evaluation (Fig. 4B), we evaluated risk levels for different stages of ice-wedge degradation/stabilization at the two study sites in northern Alaska (Table 2) based on the average thicknesses of protective layers above massive-ice bodies (including ice wedges and TCI bodies). For the PB study area, overall risk level is considered moderate (PL3 = 8.6 cm), while at the BW sites risk of degradation ranged from moderate to low (PL3 = 13.3 cm) (Table 2, Fig. 9). As expected, levels of risk in all study areas strongly depend on stages of ice-wedge degradation/stabilization: while ice wedges at UD, SA1, and SA2 stages were relatively well protected by the intermediate layer (PL3), most of the wedges at D1 and D2 stages had no protection. The data on SI1 and SI2 stages were inconsistent: almost no protection was detected at the PB study area (very high risk of degradation, despite some surficial evidence of initial

Table 2
Average thicknesses of protective layers above massive-ice bodies for different stages of ice-wedge degradation/stabilization at the northern Alaska study areas; risk levels of ice-wedge degradation were estimated according to Fig. 4 (from 1: active degradation to 6: very low risk) (for the data on individual boreholes, see Tables S1 and S2).

Stage of degradation/stabilization	Number of bore-holes, n	Water depth, cm	Thaw depth,[a] cm	Depth to permafrost table,[b] cm	Depth to massive ice, cm	Frozen protective layer (PL1),[a,c] cm	Inter-mediate layer (PL3), cm	Risk level
Prudhoe Bay, PB								
Undisturbed wedges (UD)	9	–	[37.3] ($n = 3$)	43.8	52.3	[21.7] (n = 3)	8.6	4–5
Degradation initial (D1)	10	–	[33.6] ($n = 5$)	37.7	38.5	[4.2] ($n = 5$)	0.8	2–3
Degradation advanced (D2)	4	53.3	–	49.0	49.5	–	0.5	1–2
Stabilization initial (SI1)	16	–	[45.0] ($n = 3$)	46.7	47.5	[3.7] ($n = 3$)	0.8	2–3
Stabilization initial (SI2)	8	3.3	–	49.9	49.9	–	0.0	1–2
Stabilization advanced (SA1)	8	–	[43.3] ($n = 4$)	46.5	52.1	[8.8] ($n = 4$)	5.6	3–4
Stabilization advanced (SA2)	28	–	[44.1] ($n = 24$)	51.7	72.0	[23.3] ($n = 24$)	20.3	5–6
Total	83	–	[42.2] ($n = 39$)	47.5	56.0	[17.7] ($n = 39$)	8.6	4
Barrow, BW								
Undisturbed wedges (UD)	9	–	32.7	37.4	44.7	12.0	7.2	4
Degradation initial (D1)	1	2.0	40.0	40.0	40.0	0.0	0.0	1
Degradation advanced (D2)	3	13.0	50.3	50.3	50.3	0.0	0.0	1
Stabilization initial (SI1)	4	–	38.0	40.0	45.8	7.8	5.8	3–4
Stabilization initial (SI2)	6	3.7	40.8	43.7	50.3	9.5	6.7	3–4
Stabilization advanced (SA1)	12	–	27.3	33.3	49.9	22.7	16.5	5
Stabilization advanced (SA2)	9	–	37.7	42.0	71.4	33.8	29.4	6
Total	44	–	35.7	39.4	52.7	17.5	13.3	4–5

[a] For Prudhoe Bay, average values of thaw depths and PL1 thicknesses were calculated only for boreholes drilled in the end of July 2012 [in square brackets].
[b] Top of the intermediate layer (based on the analysis of cryostructures).
[c] Thickness of frozen soil layer on top of massive ice bodies on the day of drilling (includes the frozen part of the active layer, transient layer, and intermediate layer).

stabilization), while at the BW sites the risk of degradation for these stages was from high to moderate.

Notably, ice wedges at SA2 stage in each study area generally have much better protection than wedges at UD stages (Table 2, Fig. 13). Especially thick IL above ice wedges was detected at sites where the historical imagery revealed deep and large ponds. For example, in boreholes SA6 and SA8 (PB study area) the IL thickness was 74 and 70 cm correspondingly (Fig. S11, Table S1; for location, see Fig. 2; the recent ponds were visible at the SA6 site in 1969 and 1982 aerial photographs and at the SA8 site in 1982). This increase in the IL thickness confirms our idea that the reversible process of ice-wedge degradation eventually leads to better protection and a more stable state of partially degraded ice wedges than was the case before degradation. Such wedges can be stable for a long time, until large volumes of wedge ice accumulate within the intermediate layer, increasing the risk of future degradation.

5. Discussion

5.1. Stable isotope composition of different types of ground ice and surface water

Stable oxygen and hydrogen isotopic composition of ground ice is useful for assessing the conditions during the formation of different types of ground ice and helps to differentiate ground-ice bodies of various origins (Lacelle and Vasil'chuk, 2013; Vasil'chuk and Murton, 2016). This method is very helpful for studies of ice-wedge degradation and stabilization.

The differences in isotope composition of various types of ground ice (Fig. 10) indicate differing sources of water involved in ground-ice formation. For example, in many cases ice wedges form as a result of freezing of snow-melt water, which fills frost cracks in the spring. Thus, lower $\delta^{18}O$ values indicate colder air temperatures at the time of snow accumulation. This may explain the difference between the mean values of $\delta^{18}O$ isotope for the ice wedges sampled at PB (-23.4 ± 2.1‰) and BW (-21.3 ± 1.4‰): winters at Barrow are significantly warmer, with the total annual freezing index >200 °C-day lower than at Prudhoe Bay.

Average $\delta^{18}O$ value for buried ice wedges that were sampled in the permafrost tunnel in Barrow (formed 12 to 10 ky BP, before the early Holocene Climatic Optimum), was -24.4 ± 1.8‰ ($n = 121$) (Meyer et al., 2010). The comparison of this value with the average $\delta^{18}O$ value for the active Holocene wedges from our BW study area (-21.3 ± 1.4‰) reveals a significant increase in winter air temperatures since the end of the Pleistocene (Fig. 10).

The $\delta^{18}O$ values for young ice wedges from the reestablished intermediate layer were significantly higher than values obtained from other ice wedges in PB and BW areas (Table S4): while $\delta^{18}O$ values for young wedges were -16.56‰ for PB ($n = 1$) and -17.43‰ for BW ($n = 1$), the average $\delta^{18}O$ values were -23.4 ± 2.1‰ for PB ($n = 23$) and -21.3 ± 1.4‰ for BW ($n = 15$). Since both samples of young ice were collected from ice wedges recovering after relatively deep degradation, we may presume that frost cracks could be filled not with snowmelt water, but with water accumulated in ice-wedge troughs, which is a mixture of snowmelt and rain water. The difference in $\delta^{18}O$ values also may be explained by warming climate with higher winter temperatures observed during the last decades.

In both study areas, $\delta^{18}O$ values for thermokarst-cave ice (-19.1 ± 2.5‰ for PB and -18.1 ± 1.7‰ for BW) were significantly higher than those for ice wedges (Fig. 10, Table S4). This difference can be explained by different sources of water: while ice wedges mostly form from snowmelt water, TCI forms from a mixture of snowmelt water, rain water, and water from melting ice wedges, accumulated in thermokarst troughs and underground cavities.

The $\delta^{18}O$ values for ice *belts* (layers of segregated ice) were higher than values for both ice wedges and thermokarst-cave ice bodies (Fig. 10, Table S4) because ice belts in the IL or syngenetic permafrost form from the groundwater of the active layer, which is a mixture of snowmelt and rain water. Similar $\delta^{18}O$ values for segregated ice samples were reported for the permafrost tunnel in Barrow: -16.7 ± 2.1‰ ($n = 15$) (Meyer et al., 2010).

The isotopic composition of water collected from the ice-wedge troughs was completely different for two study areas (Fig. 10): -16.0 ± 0.9‰ for PB and -10.1 ± 4.5‰ for BW. This happened because the sampling occurred at different times: in June (PB) and August (BW). Interestingly, the $\delta^{18}O$ values for sites BW-DA1, —DA2, and -DA3 (stage D2) varied from -7.0 to -8.7‰, while the value for BW-DA6 (stage D3, see Fig. S12) was -16.8‰ (Table S4). This can be explained by very active thawing of the ice wedge in this trough and especially in the adjacent thermoerosional niche, which completely changed the proportion between snowmelt water, rain water, and water from melting ice wedges, typical of water standing in thermokarst troughs. Thus, the isotopic composition of water in the ice-wedge troughs sampled by the end of the warm season indicates how active the ice-wedge degradation is, which may be used in future studies.

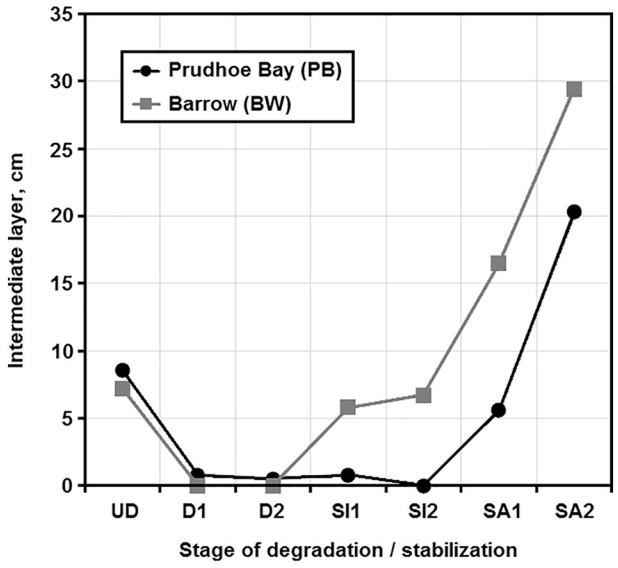

Fig. 13. Average thicknesses of the intermediate layer (PL3) above massive-ice bodies (ice wedges and TCI) for different stages of ice-wedge degradation/stabilization.

5.2. Interactions between the active layer and upper permafrost and ice-wedge degradation

Degradation of ice wedges occurs when increased seasonal soil thawing destroys the PL1 layer and reaches the top of ice wedges before the end of summer, and some summer thermal resources are spent on melting massive ice. The process of ice-wedge degradation is controlled by interactions between the active layer and upper permafrost. Leffingwell (1915) was probably the first who came to the conclusion that ice-wedge growth leads to thinning of the soil layer on top of the ice wedge. The natural process of ice-wedge lateral growth may affect ice-wedge thermokarst in one more way: the rising of growing ice wedges caused by the pressure from the adjacent soils (Leffingwell, 1915; Konishchev and Maslov, 1969; Vtyurin, 1975; Black, 1976; Romanovskii, 1977; Mackay, 1990) also leads to their thawing. Another process related to ice-wedge development that may trigger degradation is frost cracking, which increases the risk of thermal erosion along open cracks in the spring time (Fortier et al., 2007).

Definitely the active growth of ice wedges is an important factor in ice-wedge thermokarst. Tomirdiaro (1972) even assumed that formation of large and deep thaw lakes always starts when the width of large active ice wedges exceeds some critical value; then, usually after an exceptionally wet and warm summer, deep ponds form at the

crossings of large ice wedges. At the same time, many scientists have come to the conclusion that the processes of ice-wedge development may lead to periodical thawing and recovery of the top parts of ice wedges, which creates a kind of self-adjusting system (Leffingwell, 1915; Vtyurin, 1975; Romanovskii, 1977, 1993; Jorgenson et al., 2015).

To describe interactions between the active layer and upper permafrost containing ice wedges, we consider the two following models. In the first simple model, the top surface of the ice wedge coincides with the permafrost table (Fig. 14, left). This model is based on the assumptions that no interannual variations in the ALT exist, the volume of soil in the active layer above the ice wedge is constant (i.e., no sedimentation, no soil input from the rims, no accumulation of organic matter) and that no vertical deformations in the ice-wedge body occur (i.e., the pressure from the growing ice wedge leads only to deformation of the adjacent soils, which results in the rise of polygonal rims but not the wedge itself). Under these conditions, this system is completely stable, unless we take into account the further development of the ice wedge, which results in its widening caused by annual incorporation of the ice vein (A′) into the ice-wedge body and leads to thinning of the active layer (Fig. 14, right).

Based on assumption that the soil volume above the ice wedge is constant, or A1 × B1 = A2 × B2 (Fig. 14), an annual decrease in the soil thickness (B′) can be calculated from the eq

$$B' = B1 - B2 = B1 - (A1 \times B1)/A2 \quad (1)$$

Thawing of the ice wedge starts as soon as a depth of seasonal thaw exceeds B2, so the value of B' is crucial. The smaller an ice-wedge width, the larger a difference between B1 and B2. For example, if the ice wedge width (A1) is 300 cm, the ice vein width (A′) is 1 cm, and the initial active layer thickness (B1) is 40 cm, B′ will be equal 0.13 cm (Eq. 1). For a 1-m-wide ice wedge (A1 = 100 cm), B′ will be 0.4 cm. If we expand this calculation for the time period of 50 years (considering an annual formation of a new ice vein A′), a decrease in the soil thickness above the ice wedge will be very significant: 5.7 cm for the 3-m-wide wedge (initial width) and 13.3 cm for the 1-m-wide wedge. This means that according to this model the wider ice wedges are much less susceptible to thermokarst than the narrow ones.

In reality, ice-wedge thermokarst may be moderated by accumulation of new sediment. If annual accumulation of sediment is equal to B′, the ice-wedge/active layer system (Fig. 14, right) is in equilibrium; if it exceeds B′, a layer of permanently frozen soil separates the ice-wedge top surface from the active-layer base, and the wedge becomes better protected from thermokarst. Melting of ice wedges also can be compensated for by a decrease in the active-layer thickness caused by a change in climate or vegetation succession with accumulation of organic layer at the soil surface.

The simple model shown in Fig. 14 demonstrates that thinning of the soil layer on top of the ice wedge as a result of ice-wedge widening can lead to ice-wedge thawing without any external changes. But this model does not consider some factors, namely variability in the active-layer thickness related to interannual changes in weather conditions and vegetation. To describe the process of ice-wedge thermokarst more properly, we should take into account the concept of a transition zone of the upper permafrost, which consists of two layers: transient and intermediate (Shur, 1988a, 1988b; Shur et al., 2005; French and Shur, 2010) (Fig. 15).

The transient layer is a result of an interannual variability in the ALT (Shur, 1975; Shur et al., 2005). The depth of seasonal thawing varies from year to year as a result of interannual weather conditions (e.g., summer temperatures and precipitation, snow thickness). These variations lead to changes in thickness of the transient layer, that in some years is a part of the active layer and in the others a part of the permafrost. The base of the transient layer is defined by the maximum seasonal thaw (usually it occurs during warm and wet summers); in most cases the thickness of the transient layer does not exceed 30% of the average ALT (Shur et al., 2005). Only thin ice veins, composed of one or several elementary (annual) ice veins are observed within the transient layer (Fig. 15, left).

The transient layer separates ice wedges from the permafrost table. Its occurrence usually prevents ice wedges from thawing under relatively stable climate conditions, but fluctuations in weather conditions along with the thinning of the soil layer above the growing wedges eventually lead to complete thawing of the transient layer (usually during warm and wet summers), which may affect the top parts of the wedges. Several consecutive years with deep seasonal thaw may result in relatively deep thawing of the upper parts of ice wedges. Accumulation of water and snow in developing troughs causes increase in soil temperatures and stimulates additional thawing.

Much better protection of ice wedges is provided by the ice-rich intermediate layer (Shur, 1988a, 1988b; French and Shur, 2010; Shur et al., 2011; Kanevskiy et al., 2013, 2016). This layer forms as a result of a gradual decrease in the active-layer thickness, mostly as a result of accumulation of organic matter after termination or slow-down of sedimentation (Shur, 1988a, 1988b). This long-term process transforms the initial transient layer and a part of the initial active layer into a perennially frozen state. In some cases, the entire mineral part of the initial active layer joins the permafrost. Formation of the intermediate layer is a major factor of ice-wedge recovery after the thermokarst events, but if the intermediate layer is not affected by thermokarst for hundreds of years, significant volumes of wedge ice may accumulate within this layer (Fig. 15, right), which again makes this terrain vulnerable to the ice-wedge thermokarst. Thus, the intermediate layer protects ice wedges from thawing only for a limited time period, unless the active

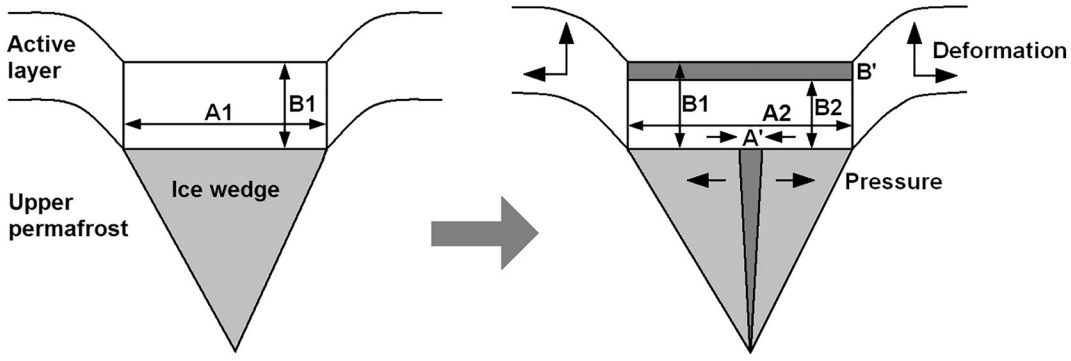

Fig. 14. Thinning of the soil layer on top of the ice wedge as a result of ice-wedge widening. Left – Initial ice wedge; right – new ice vein incorporated into the ice-wedge body. A1 – Initial width of the ice wedge; B1 – initial thickness of the active layer; A2 – width of the ice wedge after incorporation of the ice vein (A′) into the ice-wedge body; B2 – thickness of the active layer after incorporation of the ice vein.

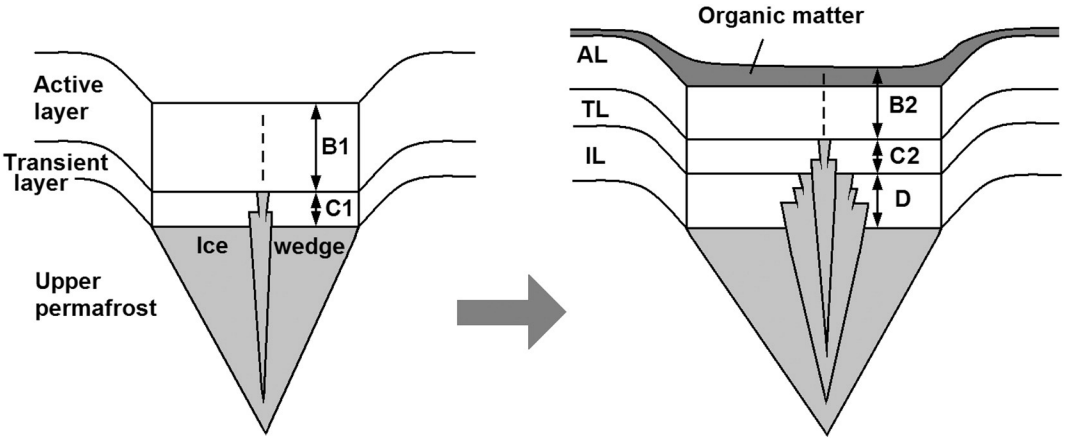

Fig. 15. Formation of transient (left image) and intermediate (right image) layers separating the main ice-wedge body from the active layer base. AL – Active layer; TL – transient layer; IL – intermediate layer; B1 – initial average thickness of the active layer; B2 – average thickness of the active layer after accumulation of organic matter; C1 – initial average thickness of the transient layer; C2 –average thickness of the transient layer after accumulation of organic matter; D – thickness of the ice-rich intermediate layer, formed as a result of transformation of the initial transient layer and the lower part of the initial active layer into a perennially frozen state triggered by a decrease in the ALT after accumulation of organic matter.

wedge-ice formation is already terminated by the time the intermediate layer forms.

The model of the active layer/upper permafrost system (Fig. 15, right) suggests that an estimation of the risk of ice-wedge thermokarst requires information on thickness and properties of protective layers overlying ice wedges, including active, transient, and intermediate layers (Fig. 4A). While thickness of PL1 (or total thickness of the frozen soil above the ice wedge, which includes the frozen part of active layer, transient layer, and intermediate layer) can be easily measured in the field, one of the main problems is measuring the ALT for the current year unless the drilling is conducted when the seasonal thawing reaches its maximum (early September for northern Alaska). Theoretically, the ALT may be measured with a permafrost probe at the drilling site at the end of the warm season, but this method is unreliable because the site may be strongly affected by the drilling itself and therefore the ALT measurements may not reflect real values under natural conditions. Thus, estimations of thickness of PL2, which includes transient and intermediate layers, in most cases cannot be precise.

The boundary between the transient and intermediate layers (or the upper boundary of PL3) in many cases can be recognized by a stark difference in cryogenic structure. The transient layer is relatively ice-poor and characterized by lenticular and reticulate cryostructures formed by thin (usually <1 or 2 mm) ice lenses. In contrast, the intermediate layer (PL3) is extremely ice-rich, with predominantly ataxitic (suspended) cryostructure and numerous thick ice layers (belts) that mark positions of former permafrost tables during the process of gradual decrease in the active-layer thickness (Shur, 1988a, 1988b; French and Shur, 2010; Kanevskiy et al., 2013). During field studies, we defined the upper ice belt as the boundary between the transient and intermediate layers.

Because the intermediate layer (PL3) provides long-term stability for ice wedges, the primary goal in studies of ice-wedge vulnerability

Table 3
Main factors affecting degradation and stabilization of ice wedges.

Factors	Degradation	Stabilization
1. Climate		
1.1. Air temperature	1. Increase in summer air temperatures usually leads to increase in ALT. 2. Increase in winter air temperatures leads to increase in soil temperature and slight increase in ALT.	1. Decrease in summer air temperatures usually leads to decrease in ALT. 2. Decrease in winter air temperatures leads to decrease in soil temperature and ALT.
1.2. Snow cover	1. Increase usually leads to increase in soil temperatures and ALT. 2. Increase may lead to flooding and/or thermal erosion. 3. Decrease leads to increase in frost-cracking activity and consequently in rates of ice-wedge development and related thinning of protective layers	1. Decrease usually leads to decrease in soil temperatures and ALT. 2. Increase leads to decrease in frost-cracking activity and consequently in rates of ice-wedge development.
1.3. Summer precipitation	1. Increase may lead to increase in soil moisture and consequent increase in ALT but may lead to decrease in ALT in the following year. 2. Increase may also lead to flooding and/or thermal erosion.	Decrease may lead to decrease in soil moisture and consequent decrease in ALT, especially in organic soils.
2. Flooding	1. Leads to increase in water depth in troughs and consequent increase in ALT. 2. May cause thermal erosion along ice wedges. 3. May cause water impoundment above polygons.	May cause additional accumulation of sediments and organic matter above ice wedges, which increases depth to ice wedges and may lead to decrease in ALT.
3. Topography	1. Sloping terrain increases risk of thermal erosion along ice wedges. 2. Flat terrain increases risk of water impoundment.	1. Sloping terrain prevents water impoundment. 2. Flat terrain reduces risk of thermal erosion.
4. Vegetation	Disturbances of vegetation or its loss lead to increase in ALT.	Fast growth of vegetation, especially moss, leads to decrease in soil temperatures and ALT; this is a main cause of the IL formation.
5. Sedimentation	Termination of sedimentation, if not compensated by fast vegetation growth, may increase risk of thermokarst caused by increasing rate of lateral ice-wedge development.	1. Fast sedimentation in troughs increases depth to ice wedges. 2. Termination of sedimentation under certain conditions leads to vegetation succession which may cause a decrease in ALT.
6. Ice-wedge development	1. Widening of ice wedges and their rising caused by pressure from adjacent soils reduces thicknesses of protective layers. 2. Accumulation of significant volumes of wedge ice in the intermediate layer results in loss of its protective role. 3. Frost cracking increases a risk of thermal erosion along open cracks in the spring time.	Development of ice wedges under thermokarst ponds leads to rising of ice wedges and adjacent soils and decrease in water depth above wedges (SA4a in Fig. 12).

to thermokarst is to detect and measure the thickness of PL3 above ice wedges in the study area. The ice content of this layer is also very important, but its influence on the process of the ice-wedge degradation is divergent. High ice content, typical of the IL, results in high thaw strain (Shur, 1988a, 1988b), which means that its complete thawing in many cases does not lead to significant increase in the ALT, but instead leads to a general surface subsidence as found by Streletskiy et al. (2016) and a decrease in total thickness of soil above ice wedges –– and therefore in their resilience to thermokarst. On the other hand, thawing of ice-rich soil at the base of the active layer occurs slowly because of the high latent heat required for fusion of ice. Thus, a complete thawing of the thick IL may occur only as a result of very significant climatic changes or serious disturbances on the surface.

5.3. Main factors of ice-wedge degradation and stabilization

The transient and intermediate layers provide good protection for ice wedges, but they cannot always prevent their thawing. Under certain conditions, a significant increase in the ALT leads to thawing of the IL and ice-wedge degradation, which may continue for years or even decades, but in most cases eventually results in ice-wedge stabilization. Interacting factors such as climate, topography, vegetation, surface and groundwater, and soil properties create positive and negative feedbacks to permafrost degradation (Jorgenson et al., 2006, 2010, 2015; Shur and Jorgenson, 2007). The main factors affecting the processes of ice-wedge degradation and stabilization are summarized in Table 3.

5.4. Quasi-cyclic process of ice-wedge degradation/stabilization

Our conceptual model (Fig. 12, Table 1) summarizes potential ways of ice-wedge evolution as a reaction to their initial degradation. Processes of ice-wedge stabilization eventually lead to complete recovery of ice wedges, which makes them vulnerable for a new cycle of ice-wedge thermokarst. In reality, recovered ice wedges (SA stages) are much better protected by thick IL than undisturbed ones (Fig. 13), and these wedges become vulnerable for thermokarst again only after active ice-wedge development within the IL over many dozens or hundreds of years. The duration of the complete recovery strongly depends on the depth and extent of ice-wedge degradation (Table 1). Though it may be difficult in many cases to differentiate undisturbed and advanced stabilization stages, recovery of degraded wedges usually does not return the ice-wedge system to its original condition so we are reluctant to characterize ice-wedge degradation/stabilization as a fully cyclic process; it is rather *quasi-cyclic*.

For example, complete degradation (stage D4) always leads to a complete rearrangement of polygonal systems, which starts with the formation of new ice wedges after thaw-lake drainage (Mackay and Burn, 2002), and we presume that deep thawing of ice wedges (stage D3) in some cases may also lead to such rearrangement. As a result, ice wedges of a new generation (stage SA3) may form completely different polygonal nets; and buried wedges of old generations, along with corresponding TCI bodies, may occur beneath the central parts of new polygons. For example, buried wedge ice was encountered under 30-cm-thick IL in the T20 borehole, which was drilled in a polygon center (PB study area, Table S1). Occurrence of buried wedge ice in the central parts of polygons may lead to underestimation of massive-ice volume because these buried ice bodies cannot be detected visually on the surface or using aerial photographs.

Our studies at PB and BW show that ice-wedge degradation usually terminates at stages D1 or D2. In many cases, it is difficult to determine without drilling if a wedge is still degrading or if its initial stabilization has already begun. Sometimes different parts of the same wedge may experience stabilization and degradation at the same time, in large part as a result of redistribution of surface water as pits develop along differing parts of the ice wedge. Transition from degradation to stabilization is always a period of uncertainty when the process can take either direction: toward recovery of the IL or to continuing degradation. The direction of further ice-wedge evolution depends on numerous factors listed above (Table 3).

We recognize that our conceptual model provides only a provisional understanding that can eventually be tested through future modeling of the interaction of the numerous biophysical factors affecting ice-wedge evolution. However, current permafrost models are insufficient at quantifying the interactions between thaw settlement, topographic changes, water redistribution, energy balance changes, nutrient dynamics, vegetation succession, peat accumulation/decomposition, and ground-ice aggradation that are all critical to understanding ice-wedge dynamics.

5.5. Ice-wedge degradation and thaw-lake formation

Thaw-lake formation resulting from complete ice-wedge degradation (stage D4 in our conceptual model) is a complex multistage process, which has been described in numerous publications (Hopkins, 1949; Soloviev, 1962; Tomirdiaro, 1972; Czudek and Demek, 1973; Shur, 1988a; Jorgenson and Shur, 2007; Shur and Osterkamp, 2007; Morgenstern et al., 2011, 2013; Shur et al., 2012; Kanevskiy et al., 2014). Most of these publications describe ice-wedge thermokarst in the areas of yedoma (the ice-rich syngenetic permafrost) (Schirrmeister et al., 2013 and references therein), which started and mainly occurred during the transition from the Pleistocene to Holocene with formation of large and deep (>20 m) thaw-lake basins and lacustrine plains.

In the areas where ice wedges are mainly epigenetic, including the Arctic Coastal Plain of Alaska, thaw lakes and lake basins are usually not deep because their depth is limited by maximum thaw settlement. For example, formation of thaw lakes >2 m deep in the Barrow area is not common, which corresponds to the ground-ice content in the upper permafrost (Sellmann et al., 1975). Potential transformation of small thermokarst pits and troughs into large thaw lakes in such areas is still debated. According to a concept of thaw-lake cycles (Hopkins, 1949; Britton, 1957; Hussey and Michelson, 1966; Billings and Peterson, 1980; Everett, 1980b; Hinkel et al., 2003), ice-wedge degradation on the Arctic Coastal Plain of Alaska triggered by climate change or surface disturbance leads to formation of large lakes; after degradation of ground ice under thaw lakes and subsequent lake drainage, the surface theoretically may return to near-original conditions as a result of ground-ice reaggradation. Jorgenson and Shur (2007) came to the conclusion that on the Arctic Coastal Plain of Alaska lake formation, drainage, and ground-ice aggradation are too slow to have allowed a complete thaw-lake cycle through the Holocene. French (2007) also did not see any clear evidence that the later stages (complete elimination of thermokarst depressions from the landscape) of the thaw-lake cycle actually exist.

The probability of formation of large thaw lakes from initial ice-wedge thermokarst is definitely <1% and possibly <0.01% (Shur and Osterkamp, 2007). According to Jorgenson et al. (2015), lake formation may occur only if ice-wedge volume is sufficient: presumably it should exceed 40%. Even in the areas with extremely ice-rich permafrost, which have experienced heavy disturbance, deep initial thermokarst depressions cannot easily transform into thaw lakes. Lawson (1986) reported that during 30 years after heavy disturbance at several drill sites in northern Alaska, no thaw lakes had formed and that in most cases the surface had been revegetated and stabilized. Shur (1988a) described numerous unsuccessful attempts to create artificial thaw lakes in the yedoma region of Siberia by removal of vegetation and surficial peat. In most cases, rates of thaw settlement slowed significantly after several years of very active thermokarst development.

We believe that the mechanism of the intermediate layer reformation, which leads to ice-wedge stabilization and recovery (Shur, 1988a; Jorgenson et al., 2006, 2015), explains this phenomenon. Our study shows that partial degradation and subsequent stabilization of ice wedges

make them better protected than before degradation because the intermediate layer is usually 2 to 3 times thicker on top of stabilized ice wedges than on top of initial ice wedges in undisturbed conditions. As a result, the likelihood of formation of large thaw lakes in the continuous permafrost zone triggered by ice-wedge degradation alone is very low.

6. Conclusions

Ice-wedge degradation and stabilization greatly depends on interactions between the active layer and the transition zone of the upper permafrost. Vulnerability of ice wedges to thermokarst is controlled by the thickness of the IL overlying ice wedges, which protects them from thawing. Degradation of ice wedges in most cases is triggered by increases in the ALT during exceptionally warm and wet summers or as a result of flooding or disturbance. The thinning of the soil layer on top of the ice wedge as a result of ice-wedge widening and the rising of the growing ice wedge caused by the pressure from the adjacent soils can also lead to ice-wedge thawing, which may occur even without any significant climate fluctuations or disturbance.

In the continuous permafrost zone, degradation of ice wedges very seldom continues to their complete melting, and in most cases wedges recover. Vegetation colonization and accumulation of organic matter in the troughs developing over degrading wedges leads to decreases in the ALT and formation of the ice-rich IL above stabilizing ice wedges. Thus, the process of ice-wedge degradation is often reversed with rejuvenation of ice wedges and formation of the new intermediate layer above ice wedges. This explains a very low probability of formation of large thaw lakes in the continuous permafrost zone as a result of ice-wedge thermokarst.

A thickness of the IL on top of stabilized ice wedges is much greater than that in undisturbed conditions. This makes the permafrost more resistant to external changes, such as climate change and disturbance. Partial degradation and subsequent stabilization of ice wedges make them better protected from thawing than before degradation. Such wedges can be very stable until large volumes of wedge ice accumulate within the intermediate layer, increasing the risk of future degradation.

Interacting factors of ice-wedge degradation and stabilization lead to more complex patterns of ice-wedge dynamics than previously described. Therefore, we modified earlier conceptual models of degradation/stabilization stages to include progressive and complete degradation of extremely ice-rich soils to the thaw-lake stage. We also identified alternative trajectories whereby degradation phases can shift to stabilization phases as a result of surface modifications and are subsequently altered by renewed ice-wedge development. Our studies at PB and BW show that in most cases ice-wedge degradation terminates at stages D1 or D2.

The comparison of the two study areas revealed that the same stages of degradation/stabilization occurred in both areas and that general trends were similar. However, differences were significant in surface and subsurface conditions, which affect processes of ice-wedge degradation/stabilization. The terrain at BW, which belongs to the old primary surface of the Arctic Coastal Plain, is better drained; and randomly distributed, water-filled isolated thermokarst pits are more common here than interconnected water-filled troughs, which are typical of PB. At BW, wedge-ice content is ~1.5 times higher than at PB, and ice-wedge degradation at BW started much earlier, as indicated by the dominance of high-centered polygons clearly visible on the 1949 aerial photos. The last major cycle of degradation/stabilization at BW started in the early 1950s and was completed in general by the early 2000s, though currently degrading ice wedges still exist in this area (~10% of ice wedges studied in 2012). At PB, widespread degradation of ice wedges started only in the late 1980s, and almost one-half of the studied ice wedges were still experiencing degradation in 2011–2012. Accordingly, stabilization of ice wedges in this area also started much later than at BW. As a result, the thicknesses of the protective intermediate layer measured for different stages of ice-wedge stabilization were significantly lower at PB than at BW.

Our conceptual model is based upon field observations on the Arctic Coastal Plain, Alaska, and applicable to lowland areas of the continuous permafrost zone. We expect that future works will encounter variations across other landscapes, which will help to identify additional processes that affect ice-wedge evolution, such as colluvial burial on slopes, differing vegetation recovery patterns, and effects of warm vs. cold permafrost.

Acknowledgements

This work was supported by the National Science Foundation grants ARC 1023623 and ArcSEES 1233854. Logistical support was provided by CH2MHill Polar Services. James 'Tripp' Collier, Karen Jorgenson, Joshua Koch, Katie Nicolato, Kimberly Wickland, Ksenia Ermokhina, Georgiy Matyshak, Jana Peirce, and Lisa Wirth participated in field work. Isotope analyses of ground ice and water were performed by Tim Howe and Norma Haubenstock, Alaska Stable Isotope Facility at the University of Alaska Fairbanks. We also acknowledge Ukpeaġvik Iñupiat Corporation (UIC) for providing access to its privately owned lands at Barrow. We would like to thank Editor Dr. Richard Marston and two anonymous reviewers for valuable comments and suggestions, which helped us to improve the paper.

Appendix A. Supplementary data

Supplementary data associated with this article can be found in the online version, at http://dx.doi.org/10.1016/j.geomorph.2017.09.001. These data include the Google map of the most important areas described in this article.

References

Abolt, C.J., Young, M.H., Caldwell, T.G., 2016. Numerical modelling of ice-wedge polygon geomorphic transition. Permafr. Periglac. Process. 28 (1):347–355. http://dx.doi.org/10.1002/ppp.1909.

Alaska Climate Research Center, University of Alaska Fairbanks, 1981-2010. Climate Normals. http://climate.gi.alaska.edu/Climate/Normals.

Billings, W.D., Peterson, K.M., 1980. Vegetational change and ice-wedge polygons through the thaw-lake cycle in Arctic Alaska. Arct. Alp. Res. 12 (4), 413–432.

Black, R.F., 1976. Periglacial features indicative of permafrost: ice and soil wedges. Quat. Res. 6, 3–26.

Black, R.F., 1983. Three superimposed systems of ice wedges at McLeod Point, northern Alaska, may span most of Wisconsinan stage and Holocene. Permafrost: Fourth International Conference Proceedings. National Academy Press, Washington, DC, pp. 68–73.

Bockheim, J.G., Hinkel, K.M., 2012. Accumulation of excess ground ice in an age sequence of drained thermokarst lake basins, Arctic Alaska. Permafr. Periglac. Process. 23 (3): 231–236. http://dx.doi.org/10.1002/ppp.1745.

Bray, M.T., French, H.M., Shur, Y., 2006. Further cryostratigraphic observations in the CRREL permafrost tunnel, Fox, Alaska. Permafr. Periglac. Process. 17 (3), 233–243.

Britton, M.E., 1957. Vegetation of the Arctic tundra. In: Hansen, H.P. (Ed.), Arctic Biology: 18th Biology Colloquium. Oregon State University Press, Corvallis, pp. 26–61.

Brown, J., 1965. Radiocarbon dating, Barrow, Alaska. Arctic 18 (1), 36–48.

Brown, J., 1967. Tundra soils formed over ice wedges, northern Alaska. Soil Sci. Soc. Am. Proc. 31 (5), 686–691.

Brown, J., 1968. An Estimation of the Volume of Ground Ice, Coastal Plain, Northern Alaska. A First Approximation. Technical Note. CRREL, Hanover, New Hampshire. p. 22.

Brown, J., 1969. Soil Properties Developed on the Complex Tundra Relief of Northern Alaska. 18. Builetyn Peryglacjalny, pp. 153–167.

Brown, J., Johnson, P.L., 1965. Pedo-ecological investigations, Barrow, Alaska. Technical Report 159. CRREL, Hanover, New Hampshire, p. 37.

Brown, J., Sellmann, P.V., 1973. Permafrost and coastal plain history of arctic Alaska. In: Britton, M.E. (Ed.), Alaskan Arctic Tundra. Technical Paper No. 25. Arctic Institute of North America, pp. 31–47.

Brown, J., Nelson, F., Romanovsky, V.E., Seybold, C., Hollister, R.D., Tweedie, C.E., 2015. Long-term observations of active layer thawing and freezing, Barrow, Alaska. 7th Canadian Permafrost Conference, September 20–23, 2015, Quebec City, Quebec, Canada.

Buchhorn, M., Raynolds, M.K., Kanevskiy, M., Matyshak, G., Shur, Y., Willis, M.D., Peirce, J.L., Wirth, L.M., Walker, D.A., 2016. Effects of 45 years of heavy road traffic and climate change on the thermal regime of permafrost and tundra at Prudhoe Bay, Alaska. Abstracts of the Eleventh International Conference on Permafrost, June 20–24, 2016, Potsdam, Germany, pp. 1221–1222.

Christiansen, H.H., Matsuoka, N., Watanabe, T., 2016. Progress in understanding the dynamics, internal structure and palaeoenvironmental potential of ice wedges and

sand wedges. Permafr. Periglac. Process. 27 (4):365–376. http://dx.doi.org/10.1002/ppp.1920.
Craig, H., 1961. Standard for reporting concentrations of deuterium and oxygen-18 in natural waters. Science 133, 1833–1834.
Czudek, T., Demek, J., 1973. Thermokarst in Siberia and its influence on the development of lowland relief. Quat. Res. 1, 103–120.
De Klerk, P., Donner, N., Karpov, N.S., Minke, M., Joosten, H., 2011. Short-term dynamics of a low-centred ice-wedge polygon near Chokurdakh (NE Yakutia, NE Siberia) and climate change during the last ca 1250 years. Quat. Sci. Rev. 30:3013–3031. http://dx.doi.org/10.1016/j.quascirev.2011.06.016.
Everett, K.R., 1980a. Geology and permafrost. In: Walker, D.A., Everett, K.R., Webber, P.J., Brown, J. (Eds.), Geobotanical Atlas of the Prudhoe Bay Region, Alaska. CRREL Report 80-14. U.S. Army Corps of Engineers, Cold Regions Research and Engineering Laboratory, Hanover, NH, pp. 8–9.
Everett, K.R., 1980b. Landforms. In: Walker, D.A., Everett, K.R., Webber, P.J., Brown, J. (Eds.), Geobotanical Atlas of the Prudhoe Bay Region, Alaska. CRREL Report 80-14. U.S. Army Corps of Engineers, Cold Regions Research and Engineering Laboratory, Hanover, NH, pp. 14–19.
Farquharson, L.M., Mann, D.H., Grosse, G., Jones, B.M., Romanovsky, V.E., 2016. Spatial distribution of thermokarst terrain in Arctic Alaska. Geomorphology 273:116–133. http://dx.doi.org/10.1016/j.geomorph.2016.08.007.
Fedorov, A.N., Gavriliev, P.P., Konstantinov, P.Ya., Hiyama, T., Iijima, Y., Iwahana, G., 2012. Contribution of thawing permafrost and ground ice to the water balance of young thermokarst lakes in Central Yakutia. In: Melnikov, V.P. (Ed.), In Proceedings of the Tenth International Conference on Permafrost, June 25–29, 2012, Salekhard, Russia. Vol. 2 Translations of Russian Contributions. The Northern Publisher, Salekhard, Russia, pp. 75–80.
Fortier, D., Allard, M., Shur, Y., 2007. Observation of rapid drainage system development by thermal erosion of ice wedges on Bylot Island, Canadian Arctic archipelago. Permafr. Periglac. Process. 18 (3), 229–243.
Fortier, D., Kanevskiy, M., Shur, Y., 2008. Genesis of reticulate-chaotic cryostructure in permafrost. In: Proceedings of the Ninth International Conference on Permafrost, June 29 – July 3, 2008, Fairbanks, Alaska. Kane, D.L. & Hinkel, K.M. (Eds). Institute of Northern Engineering, University of Alaska Fairbanks, vol. 1, pp. 451–456.
French, H.M., 2007. The Periglacial Environment. 3rd ed. John Wiley and Sons Ltd., Chichester, UK, p. 458.
French, H., Shur, Y., 2010. The principles of cryostratigraphy. Earth Sci. Rev. 110:190–206. http://dx.doi.org/10.1016/j.earscirev.2010.04.002.
Frost, G.V., Macander, M.J., Liljedahl, A.K., Walker, D.A., 2014. Regional patterns of ice-wedge degradation since the mid-20th century across northern Alaska. Book of Poster Abstracts, Arctic Change 2014 Conference, Ottawa, Canada, 8-12 December, p. 58.
Gamon, J.A., Kershaw, G.P., Williamson, S., Hik, D.S., 2012. Microtopographic patterns in an arctic baydjarakh field: do fine-grain patterns enforce landscape stability? Environ. Res. Lett. 7, 015502. http://dx.doi.org/10.1088/1748-9326/7/1/015502.
Godin, E., Fortier, D., Coulombe, S., 2014. Effects of thermo-erosion gullying on hydrologic flow networks, discharge and soil loss. Environ. Res. Lett. 9:105010. http://dx.doi.org/10.1088/1748-9326/9/10/105010.
Gold, L.W., Lachenbruch, A.H., 1973. Thermal conditions in permafrost. A Review of the North American Literature. In North American Contribution to the Second International Conference on Permafrost. Washington, D.C., pp. 3–23
Helbig, M., Boike, J., Langer, M., Schreiber, P., Runkle, B.R.K., Kutzbach, L., 2013. Spatial and seasonal variability of polygonal tundra water balance: Lena River Delta, northern Siberia (Russia). Hydrogeol. J. 21 (1):133–147. http://dx.doi.org/10.1007/s10040-012-0933-4.
Hinkel, K.M., Nelson, F.E., Shur, Y., Brown, J., Everett, K.R., 1996. Temporal changes in moisture content of the active layer and near-surface permafrost at Barrow, Alaska, USA: 1962–1994. Arct. Alp. Res. 28 (3), 300–310.
Hinkel, K.M., Eisner, W.R., Bockheim, J.G., Nelson, F.E., Peterson, K.M., Dai, X., 2003. Spatial extent, age, and carbon stocks in drained thaw lake basins on the Barrow Peninsula, Alaska. Arct. Antarct. Alp. Res. 35 (3), 291–300.
Hopkins, D.M., 1949. Thaw lakes and thaw sinks in the Imuruk Lake area, Seward Peninsula, Alaska. J. Geol. 57, 119–131.
Hussey, K.M., Michelson, R.W., 1966. Tundra relief features near Point Barrow, Alaska. Arctic 19 (2), 162–184.
Jones, B.M., Grosse, G., Arp, C.D., Liu, L., Miller, E.A., Hayes, D.J., Larsen, C., 2015. Recent arctic tundra fire initiates widespread thermokarst development. Sci Rep 5:15865. http://dx.doi.org/10.1038/srep15865.
Jorgenson, M.T., 2011. Coastal region of northern Alaska, Guidebook to permafrost and related features. Alaska Division of Geological & Geophysical Surveys Guidebook 10, p. 188 (pp).
Jorgenson, M.T., Grosse, G., 2016. Remote sensing of landscape change in permafrost regions. Permafr. Periglac. Process. 27 (4):324–338. http://dx.doi.org/10.1002/ppp.1914.
Jorgenson, M.T., Shur, Y., 2007. Evolution of lakes and basins in northern Alaska and discussion of the thaw lake cycle. J. Geophys. Res. 112, F02S17. http://dx.doi.org/10.1029/2006JF000531.
Jorgenson, M.T., Shur, Y.L., Pullman, E.R., 2006. Abrupt increase in permafrost degradation in Arctic Alaska. Geophys. Res. Lett. 25 (2), L02503.
Jorgenson, T., Shur, Y.L., Osterkamp, T.E., 2008. Thermokarst in Alaska. In: Proceedings of the Ninth International Conference on Permafrost, Vol. 1, June 29–July 3, 2008, Fairbanks, Alaska, Kane, D.L., Hinkel, K.M. (Eds). Institute of Northern Engineering, University of Alaska Fairbanks, pp. 869–876.
Jorgenson, M.T., Romanovsky, V.E., Harden, J.W., Shur, Y., O'Donnell, J.A., Schuur, E.A.G., Kanevskiy, M.Z., 2010. Resilience and vulnerability of permafrost to climate change. Can. J. For. Res. 40, 1219–1236.
Jorgenson, T., Kanevskiy, M.Z., Shur, Y., Moskalenko, N.G., Brown, D.R.N., Wickland, K., Striegl, R., Koch, J., 2015. Ground ice dynamics and ecological feedbacks control ice-wedge degradation and stabilization. JGR Earth Surface 120 (11):2280–2297. http://dx.doi.org/10.1002/2015JF003602.
Kanevskiy, M., Fortier, D., Shur, Y., Bray, M., Jorgenson, T., 2008. Detailed cryostratigraphic studies of syngenetic permafrost in the winze of the CRREL Permafrost Tunnel, Fox, Alaska. In: Proceedings of the Ninth International Conference on Permafrost, June 29 – July 3, 2008, Fairbanks, Alaska. Kane, D.L., and Hinkel, K.M. (Eds). Institute of Northern Engineering, University of Alaska Fairbanks, vol. 1, pp. 889–894.
Kanevskiy, M.Z., Shur, Y., Jorgenson, M.T., Ping, C.-L., Michaelson, G.J., Fortier, D., Stephani, E., Dillon, M., Tumskoy, V., 2013. Ground ice in the upper permafrost of the Beaufort Sea coast of Alaska. Cold Reg. Sci. Technol. 85:56–70. http://dx.doi.org/10.1016/j.coldregions.2012.08.002.
Kanevskiy, M., Jorgenson, M.T., Shur, Y., O'Donnell, J.A., Harden, J.W., Zhuang, Q., Fortier, D., 2014. Cryostratigraphy and permafrost evolution in lacustrine lowlands of west-central Alaska. Permafr. Periglac. Process. 25 (1):14–34. http://dx.doi.org/10.1002/ppp.1800.
Kanevskiy, M., Shur, Y., Walker, D.A., Buchhorn, M., Jorgenson, T., Matyshak, G., Raynolds, M.K., Peirce, J.L., Wirth, L.M., 2016. Evaluation of risk of ice-wedge degradation, Prudhoe Bay Oilfield, AK. Abstracts of the Eleventh International Conference on Permafrost, June 20–24, 2016, Potsdam, Germany, pp. 1007–1009.
Kershaw, G.P., 2008. Snow and temperature relationships on polygonal peat plateaus, Churchill, Manitoba, Canada. In: Kane, D.L., Hinkel, K.M. (Eds.), Proceedings of the Ninth International Conference on Permafrost, Vol. 1, June 29–July 3, 2008, Fairbanks, Alaska. University of Alaska Fairbanks, Institute of Northern Engineering, pp. 925–930.
Kokelj, S.V., Jorgenson, M.T., 2013. Advances in thermokarst research. Permafr. Periglac. Process. 24 (2):108–119. http://dx.doi.org/10.1002/ppp.1779.
Kokelj, S.V., Lantz, T.C., Wolfe, S.A., Kanigan, J.C., Morse, P.D., Coutts, R., Molina-Giraldo, N., Burn, C.R., 2014. Distribution and activity of ice wedges across the forest-tundra transition, Western Arctic Canada. Journal of Geophysical Research: Earth Surface 119 (9):2032–2047. http://dx.doi.org/10.1002/2014JF003085.
Konishchev, V.N., Maslov, A.D., 1969. Fizicheskiye prichiny frontal'nogo rosta syngeneticheskikh polygonal'no-zhil'nykh l'dov [Physical causes of the frontal growth of syngenetic ice wedges]. Problemy Kriolitologii [Problems of Cryolithology] 1, 24–33 (in Russian).
Lacelle, D., Vasil'chuk, Y.K., 2013. Recent progress (2007–2012) in permafrost isotope geochemistry. Permafr. Periglac. Process. 24 (2):138–145. http://dx.doi.org/10.1002/ppp.1768.
Lachenbruch, A.H., Sass, J.H., Lawver, L.A., Brewer, M.C., Marshall, B.V., Munroe, R.J., Kennelly Jr., J.P., Galanis Jr., S.P., Moses Jr., T.H., 1988. Temperature and depth of permafrost on the Arctic slope of Alaska. In: Gryc, G. (Ed.), Geology and exploration of the National Petroleum Reserve in Alaska, 1974 to 1982: U.S. Geological Survey Professional Paper. 1399, pp. 645–656.
Lara, M.J., McGuire, A.D., Euskirchen, E.S., Tweedie, C.E., Hinkel, K.M., Skurikhin, A.N., Romanovsky, V.E., Grosse, G., Bolton, W.R., Genet, E., 2015. Polygonal tundra geomorphological change in response to warming alters future CO_2 and CH4 flux on the Barrow Peninsula. Glob. Chang. Biol. 21:1634–1651. http://dx.doi.org/10.1111/gcb.12757.
Lawson, D.E., 1986. Response of permafrost terrain to disturbance: a synthesis of observations from northern Alaska, U.S.A. Arct. Alp. Res. 18 (1), 1–17.
Leffingwell, E. de K., 1915. Ground-ice wedges, the dominant form of ground-ice on the north coast of Alaska. J. Geol. 23, 635–654.
Leffingwell, E. de K., 1919. The Canning River region, northern Alaska. U.S. Geological Survey Professional Paper 109. United States Government Printing Office, Washington, p. 251.
Liljedahl, A.K., Hinzman, L.D., Schulla, J., 2012. Ice-wedge polygon type controls low-gradient watershed-scale hydrology. In: Hinkel, K.M. (Ed.), In Proceedings of the Tenth International Conference on Permafrost Vol. 1: International Contributions. The Northern Publisher, Salekhard, Russia, pp. 231–236.
Liljedahl, A.K., Boike, J., Daanen, R.P., Fedorov, A.N., Frost, G.V., Grosse, G., Hinzman, L.D., Iijma, Y., Jorgenson, J.C., Matveyeva, N., Necsoiu, M., Raynolds, M.K., Romanovsky, V.E., Schulla, J., Tape, K.D., Walker, D.A., Wilson, C.J., Yabuki, H., Zona, D., 2016. Pan-Arctic ice-wedge degradation in warming permafrost and its influence on tundra hydrology. Nat. Geosci. 9:312–318. http://dx.doi.org/10.1038/ngeo2674.
Mackay, J.R., 1972. The world of underground ice. Ann. Assoc. Am. Geogr. 62 (1), 1–22.
Mackay, J.R., 1990. Some observations on the growth and deformation of epigenetic, syngenetic and anti-syngenetic ice wedges. Permafr. Periglac. Process. 1, 15–29.
Mackay, J.R., 1997. A full-scale field experiment (1978–1995) on the growth of permafrost by means of lake drainage, western Arctic coast: a discussion of the method and some results. Can. J. Earth Sci. 34, 17–33.
Mackay, J.R., 2000. Thermally induced movements in ice-wedge polygons, western Arctic coast: a long-term study. Geographie Physique et Quaternaire 54 (1), 41–68.
Mackay, J.R., Burn, C.R., 2002. The first 20 years (1978–1979 to 1998–1999) of ice-wedge growth at the Illisarvik experimental drained lake site, western Arctic coast, Canada. Can. J. Earth Sci. 39, 95–111.
Meyer, H., Schirrmeister, L., Andreev, A., Wagner, D., Hubberten, H.-W., Yoshikawa, K., Bobrov, A., Wetterich, S., Opel, T., Kandiano, E., Brown, J., 2010. Lateglacial and Holocene isotopic and environmental history of northern coastal Alaska — results from a buried ice-wedge system at Barrow. Quat. Sci. Rev. 29, 3720–3735.
Minke, M., Donner, N., Karpov, N., de Klerk, P., Joosten, H., 2009. Patterns in vegetation composition, surface height and thaw depth in polygon mires in the Yakutian Arctic (NE Siberia): a microtopographical characterisation of the active layer. Permafr. Periglac. Process. 20:357–368. http://dx.doi.org/10.1002/ppp.663.
Morgenstern, A., Grosse, G., Günther, F., Fedorova, I., Schirrmeister, L., 2011. Spatial analyses of thermokarst lakes and basins in Yedoma landscapes of the Lena Delta. Cryosphere 5, 849–867.

Morgenstern, A., Ulrich, M., Günther, F., Roessler, S., Fedorova, I.V., Rudaya, N.A., Wetterich, S., Boike, J., Schirrmeister, L., 2013. Evolution of thermokarst in East Siberian ice-rich permafrost: a case study. Geomorphology 201, 363–379.

Murton, J.B., 2013. Ground ice and cryostratigraphy. In Treatise on Geomorphology, Vol. 8, Glacial and Periglacial Geomorphology, Schoder, J.F. (editor-in-chief), Giardino, R., Harboor, J. (volume eds). Academic Press, San Diego, pp. 173–201.

Necsoiu, M., Dinwiddie, C.L., Walter, G.R., Larsen, A., Stothoff, S.A., 2013. Multi-temporal image analysis of historical aerial photographs and recent satellite imagery reveals evolution of water body surface area and polygonal terrain morphology in Kobuk Valley National Park, Alaska. Environ. Res. Lett. 8 (2), 025007.

O'Sullivan, J.B., 1961. Quaternary Geology of the Arctic Coastal Plain, Northern Alaska. PhD thesis, Iowa State University, Ames. p. 191.

PLANTS Database, d. Natural Resources Conservation Service, USDAhttps://plants.usda.gov.

Pollard, W., French, H.M., 1980. A first approximation of the volume of ground ice, Richards Island, Pleistocene Mackenzie delta, Northwest Territories, Canada. Can. Geotech. J. 17, 509–516.

Pollard, W., Ward, M., Becker, M., 2015. The Eureka Sound lowlands: an ice-rich permafrost landscape in transition. 7th Canadian Permafrost Conference, September 20–23, 2015, Quebec City, Quebec, Canada.

Rawlinson, S.E., 1993. Surficial geology and morphology of the Alaskan central Arctic Coastal Plain. Alaska Division of Geological & Geophysical Surveys Report of Investigation 93-1, Fairbanks, p. 172.

Raynolds, M.K., Walker, D.A., Ambrosius, K.J., Brown, J., Everett, K.R., Kanevskiy, M., Kofinas, G.P., Romanovsky, V.E., Shur, Y., Webber, P.J., 2014. Cumulative geoecological effects of 62 years of infrastructure and climate change in ice-rich permafrost landscapes, Prudhoe Bay Oilfield, Alaska. Glob. Chang. Biol. 20 (4):1211–1224. http://dx.doi.org/10.1111/gcd.12500.

Romanovskii, N.N., 1977. Formirovanie poligonal'no-zhil'nykh struktur [Formation of polygonal-wedge structures], Kondratieva, K.A. (Ed.). Nauka, Novosibirsk. p. 215 (in Russian).

Romanovskii, N.N., 1993. Osnovy Kriogeneza Litosfery [Fundamentals of Cryogenesis of Lithosphere]. Moscow University Press, Moscow, p. 336 (in Russian).

Romanovsky, V.E., Smith, S.L., Isaksen, K., Shiklomanov, N.I., Streletskiy, D.A., Kholodov, A.L., Christiansen, H.H., Drozdov, D.S., Malkova, G.V., Marchenko, S.S., 2016. Terrestrial permafrost [in "State of the climate in 2015"]. Bulletin of the American Meteorological Society, August 2016, pp. S149–S152.

Schirrmeister, L., Froese, D., Tumskoy, V., Grosse, G., Wetterich, S., 2013. Yedoma: Late Pleistocene ice-rich syngenetic permafrost of Beringia. Encyclopedia of Quaternary Science, Second edition, pp. 542–552.

Sejourne, A., Costard, F., Fedorov, A., Gargani, J., Skorve, J., Massé, M., Mège, D., 2015. Evolution of the banks of thermokarst lakes in central Yakutia (Central Siberia) due to retrogressive thaw slump activity controlled by insolation. Geomorphology 241, 31–40.

Sellmann, P.V., Brown, J., Lewellen, R.I., McKim, H.L., Merry, C.J., 1975. The classification and geomorphic implications of thaw lakes on the Arctic Coastal Plain, Alaska. Research Report 344, CRREL, Hanover, New Hampshire, p. 21.

Shiklomanov, N., Streletskiy, D., Nelson, F., 2012. Northern hemisphere component of the Global Circumpolar Active Layer Monitoring (CALM) Program. In: Proceedings of the Tenth International Conference on Permafrost, June 25–29, 2012, Salekhard, Russia. The Northern Publisher, Salekhard, Russia. Vol. 1: International Contributions. Hinkel, K.M. (Ed.), pp. 377–382.

Shumskii, P.A., 1959. Ground (subsurface) ice. Principles of Geocryology, Part I, General Geocryology. Academy of Sciences of the USSR, Moscow, pp. 274–327. Chapter IX. (in Russian) (English translation: C. de Leuchtenberg), 1964. National Research Council of Canada, Ottawa, Technical Translation 1130, p. 118.

Shur, Y.L., 1975. O perekhodnom sloye [On the transient layer]. In Metody geokriologicheskikh issledovaniy [Methods of Permafrost Studies]. Moscow, VSEGINGEO. pp. 82–85.

Shur, Y.L., 1988a. Verkhniy gorizont tolshchi merzlykh porod i termokarst [Upper horizon of permafrost and thermokarst], Pavlov, A.V. (Ed.). Nauka: Novosibirsk, 210 pp. (in Russian).

Shur, Y.L., 1988b. The upper horizon of permafrost soils. In Proceedings of the Fifth International Conference on Permafrost, Vol. 1, Senneset, K. (Ed.). Tapir Publishers, Trondheim, Norway, pp. 867–871.

Shur, Y.L., Jorgenson, M.T., 2007. Patterns of permafrost formation and degradation in relation to climate and ecosystems. Permafr. Periglac. Process. 18:7–19. http://dx.doi.org/10.1002/ppp.582.

Shur, Y., Osterkamp, T., 2007. Thermokarst. Report INE 06.11. University of Alaska Fairbanks, Institute of Northern Engineering, Fairbanks, Alaska. p. 50.

Shur, Y.L., French, H.M., Bray, M.T., Anderson, D.A., 2004. Syngenetic permafrost growth: Cryostratigraphic observations from the CRREL tunnel near Fairbanks, Alaska. Permafr. Periglac. Process. 15 (4), 339–347.

Shur, Y., Hinkel, K.M., Nelson, F.E., 2005. The transient layer: implications for geocryology and climate-change science. Permafr. Periglac. Process. 16 (1), 5–17.

Shur, Y., Jorgenson, M.T., Kanevskiy, M.Z., 2011. Permafrost. In: Singh, V.P., Singh, P., Haritashya, U.K. (Eds.), Encyclopedia of Earth Sciences Series, Encyclopedia of Snow, Ice and Glaciers. Springer, Dordrecht, The Netherlands:pp. 841–848 http://dx.doi.org/10.1007/978-90-481-2642-2.

Shur, Y., Kanevskiy, M., Jorgenson, T., Dillon, M., Stephani, E., Bray, M., 2012. Permafrost degradation and thaw settlement under lakes in yedoma environment. In Proceedings of the Tenth International Conference on Permafrost, June 25–29, 2012, Salekhard, Russia. Vol. 1 International Contributions, Hinkel, K.M. (Ed.). The Northern Publisher: Salekhard, Russia, pp. 383–388.

Smith, S.L., Romanovsky, V.E., Lewkowicz, A.G., Burn, C.R., Allard, M., Clow, G.D., Yoshikawa, K., Throop, J., 2010. Thermal state of permafrost in North America: a contribution to the International Polar Year. Permafr. Periglac. Process. 21:117–135. http://dx.doi.org/10.1002/ppp.690.

Soloviev, P.A., 1962. Alasniy relief Tsentral'noy Yakutii i ego proiskhozhdenie [Alas relief of Central Yakutia and its origin]. In: Grave, N.A. (Ed.), Mnogoletnemyorzlye Porody I Soputstvuyushchie Im Yavleniya na Territirii Yakutskoy ASSR [Permafrost and Related Features in Central Yakutia]. The Academy of Sciences of the USSR Press, Moscow, pp. 38–54 (in Russian).

Steedman, A.E., Lantz, T.C., Kokelj, S.V., 2017. Spatio-temporal variation in high-centre polygons and ice-wedge melt ponds, Tuktoyaktuk coastlands, Northwest Territories. Permafr. Periglac. Process. 28 (1):66–78. http://dx.doi.org/10.1002/ppp.1880.

Streletskiy, D.A., Shiklomanov, N.I., Nelson, F.E., Klene, A.E., 2008. Thirteen years of observations at Alaskan CALM sites: long-term active layer and ground surface temperature trends. In: Proceedings of the Ninth International Conference on Permafrost, June 29–July 3, 2008, Fairbanks, Alaska. Kane, D.L., and Hinkel, K.M. (Eds). Institute of Northern Engineering, University of Alaska Fairbanks, Vol 2, pp. 1727–1732.

Streletskiy, D.A., Shiklomanov, N.I., Little, J.D., Nelson, F.E., Brown, J., Nyland, K.E., Klene, A.E., 2016. Short communication: Thaw subsidence in undisturbed tundra landscapes, Barrow, Alaska, 1962–2015. Permafr. Periglac. Process. http://dx.doi.org/10.1002/ppp.1918.

Swanson, D., 2016. Stability of Ice-wedges in Kobuk Valley National Park and the Noatak National Preserve, 1951-2009. Natural Resource Report NPS/ARCN/NRR—2016/1248. http://dx.doi.org/10.13140/RG.2.2.28422.16966.

Tomirdiaro, S.V., 1972. Vechnaya Merzlota I Osvoenie Gornykh Stran I Nizmennostey [Permafrost and Development in Mountain Regions and Lowlands]. Magadan Publisher, Magadan 174. (in Russian).

Vasil'chuk, Y.K., Murton, J.B., 2016. Stable Isotope Geochemistry of Massive Ice. Geography. Environment. Sustainability. 03 (09), 4–23. http://dx.doi.org/10.15356/2071-9388_03v09_2016_01.

Vtyurin, B.I., 1975. Podzemnye I'dy SSSR [Ground Ice of the USSR]. Nauka, Moscow 215. (in Russian).

Walker, D.A., 1985. Vegetation and Environmental Gradients of the Prudhoe Bay Region, Alaska, CRREL Report 85–14. U.S. Army Corps of Engineers, Cold Regions Research and Engineering Laboratory, Hanover, NH, p. 240.

Walker, D.A., Everett, K.R., 1991. Loess ecosystems of northern Alaska: regional gradient and toposequence at Prudhoe Bay. Ecol. Monogr. 61 (4):437–464. http://dx.doi.org/10.2307/2937050.

Walker, D.A., Everett, K.R., Webber, P.J., Brown, J., 1980. Geobotanical Atlas of the Prudhoe Bay Region, Alaska. CRREL Report 80-14. U.S. Army Corps of Engineers, Cold Regions Research and Engineering Laboratory, Hanover, NH, p. 68.

Walker, D.A., Webber, P.J., Binnian, E.F., Everett, K.R., Lederer, N.D., Nordstrand, E.A., Walker, M.D., 1987. Cumulative impacts of oil fields on northern Alaskan landscapes. Science 238 (4828), 757–761.

Walker, D.A., Raynolds, M.K., Shur, Y., Kanevskiy, M., Ambrosius, K.J., Romanovsky, V.E., Kofinas, G.P., Brown, J., Everett, K.R., Webber, P.J., Buchhorn, M., Matyshak, G.V., Wirth, L.M., 2014. In: Walker, D.A., Raynolds, M.K., Buchhorn, M., Peirce, J.L. (Eds.), Landscape and permafrost changes in the Prudhoe Bay Oilfield, Alaska. Alaska Geobotany Center Publication AGC 14-01. University of Alaska Fairbanks, Fairbanks, AK, p. 84.

Walker, D.A., Buchhorn, M., Kanevskiy, M., Matyshak, G.V., Raynolds, M.K., Shur, Y., Wirth, L.M., 2015. In: Walker, D.A., Raynolds, M.K., Buchhorn, M., Peirce, J.L. (Eds.), Infrastructure-thermokarst-soil-vegetation interactions at Lake Colleen Site A, Prudhoe Bay, Alaska. Alaska Geobotany Center Data Report AGC 15-01. Institute of Arctic Biology, University of Alaska Fairbanks, Fairbanks, AK, p. 92.

Walker, M.D., 1990. Vegetation and floristics of pingos, Central Arctic Coastal Plain. Alaska. Dissertationes Botanicae 149.

Wolter, J., Lantuit, H., Fritz, M., Macias-Fauria, M., Myers-Smith, I., Herzschuh, U., 2016. Vegetation composition and shrub extent on the Yukon coast, Canada, are strongly linked to ice-wedge polygon degradation. Polar Res. 35 (1):27489. http://dx.doi.org/10.3402/polar.v35.27489.